Article

Current Biology

The preoptic area and dorsal habenula jointly support homeostatic navigation in larval zebrafish

Graphical abstract

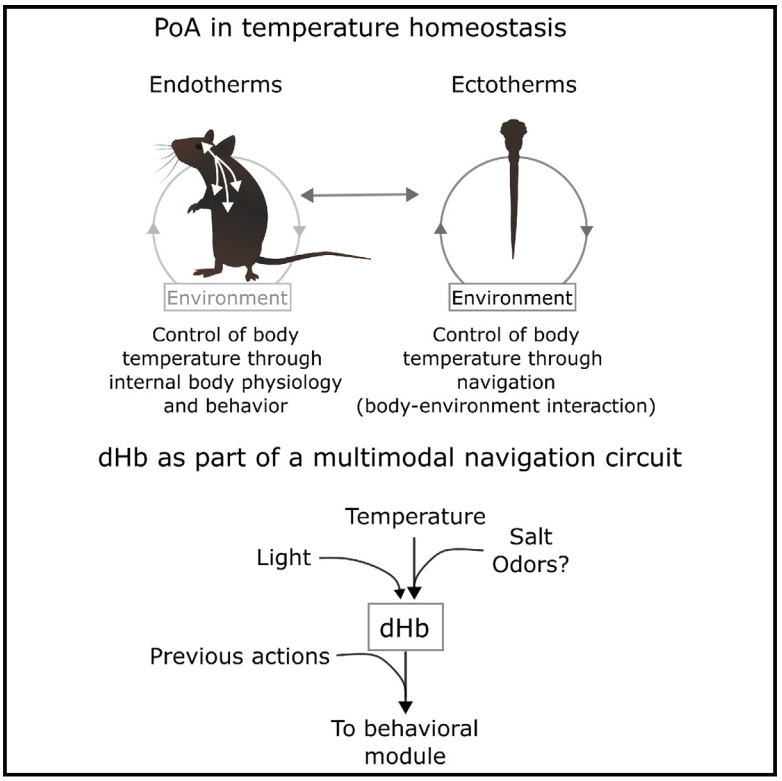

Highlights

- Larval zebrafish do homeostatic navigation by modulating turns and forward swims
- The preoptic area modulates non-directional turning vs. forward swimming
- The dorsal habenula links motor and sensory history to generate directional turns
- This circuit also conveys relative valence of stimuli to perform homeostatic navigation

Authors

Virginia Palieri, Emanuele Paoli, You Kure Wu, Martin Haesemeyer, Ilona C. Grunwald Kadow, Ruben Portugues

Correspondence

ilona.grunwald@ukbonn.de (I.C.G.K.), ruben.portugues@tum.de (R.P.)

In brief

Palieri et al. show that larval zebrafish maintain body temperature by combining a non-directional strategy with directional navigation. A whole-brain functional screen identifies a circuit involved in this behavior. The preoptic area modulates non-directional turning probability, while the dorsal habenula is required for coherent directional turns.

Palieri et al., 2024, Current Biology *34*, 489–504
February 5, 2024
https://doi.org/10.1016/j.cub.2023.12.030

CellPress

Current Biology

CellPress
OPEN ACCESS

Article

The preoptic area and dorsal habenula jointly support homeostatic navigation in larval zebrafish

Virginia Palieri,[1,2,6] Emanuele Paoli,[1,6] You Kure Wu,[1] Martin Haesemeyer,[3] Ilona C. Grunwald Kadow,[2,4,7,*] and Ruben Portugues[1,5,8,9,*]

[1]Institute of Neuroscience, Technical University of Munich, Biedersteiner Strasse 29, 80802 Munich, Germany
[2]School of Life Sciences, Technical University of Munich, Freising, Germany
[3]Department of Neuroscience, The Ohio State University College of Medicine, Columbus, OH 43210, USA
[4]Institute of Physiology II, University of Bonn, Medical Faculty (UKB), Nussallee 11, 53115 Bonn, Germany
[5]Munich Cluster of Systems Neurology (SyNergy), Feodor-Lynen-Str. 17, 81377 Munich, Germany
[6]These authors contributed equally
[7]X (formerly Twitter): @ikadow
[8]X (formerly Twitter): @PortuguesLab
[9]Lead contact
*Correspondence: ilona.grunwald@ukbonn.de (I.C.G.K.), ruben.portugues@tum.de (R.P.)
https://doi.org/10.1016/j.cub.2023.12.030

SUMMARY

Animals must maintain physiological processes within an optimal temperature range despite changes in their environment. Through behavioral assays, whole-brain functional imaging, and neural ablations, we show that larval zebrafish, an ectothermic vertebrate, achieves thermoregulation through homeostatic navigation—non-directional and directional movements toward the temperature closest to its physiological setpoint. A brain-wide circuit encompassing several brain regions enables this behavior. We identified the preoptic area of the hypothalamus (PoA) as a key brain structure in triggering non-directional reorientation when thermal conditions are worsening. This result shows an evolutionary conserved role of the PoA as principal thermoregulator of the brain also in ectotherms. We further show that the habenula (Hb)-interpeduncular nucleus (IPN) circuit retains a short-term memory of the sensory history to support the generation of coherent directed movements even in the absence of continuous sensory cues. We finally provide evidence that this circuit may not be exclusive for temperature but may convey a more abstract representation of relative valence of physiologically meaningful stimuli regardless of their specific identity to enable homeostatic navigation.

INTRODUCTION

In response to environmental perturbations, animals relocate to maintain their physiological processes within a healthy range (i.e., homeostasis).[1] Regardless of the specific strategy and environmental factors involved, the nervous system plays a crucial role during homeostasis by tracking environmental and internal signals and comparing them with past and ongoing sensory-evoked experiences and physiological states.[2] Temperature is a prototypical example of how an environmental factor can critically affect the physiological processes in all organisms.[3] A failure to assess its absolute level, rate of change, and derived valence can have a variety of consequences, from tissue damage to failure of the entire system.[3–5] Endotherms, such as mammals, can couple volitional behavioral strategies—for example, warm- or cold-seeking behavior—with autonomic measures, such as shivering/sweating or vasoconstriction/vasodilation,[6] to cope with thermal stress. On the contrary, ectotherms, such as fish, amphibians, and reptiles, lack an autonomic homeostatic mechanism to regulate their body temperature.[7] These animals need to move in order to navigate toward places where the external temperature matches their homeostatic setpoint.[8] Thus, for ectotherms, thermoregulation is achieved mainly through navigation. We will refer to this phenomenon as homeostatic navigation.

Despite extensive research into the behavioral strategies and brain regions involved in either navigation or homeostasis, the way these two processes interact and how the nervous system supports homeostatic navigation is poorly understood. Notably, it is an open question whether brain areas such as the preoptic area of the hypothalamus (PoA), which regulates temperature homeostasis in endotherms and has a role in behavioral fever and temperature perception in ectotherms,[9,10] could also be involved in homeostatic navigation.

In this study, we dissect the characteristics and neural mechanisms of homeostatic navigation in larval zebrafish using a combination of spatial, temporal, and virtual thermal gradients. We show that fish modulate their reorientation probability and direction of turning based on their sensory context and previous motor choices. In this way, when the context worsens (i.e., moves away from the physiological temperature setpoint), the reorientation probability significantly increases and fish favor coherent, steering reversal maneuvers over random turns or immobility.

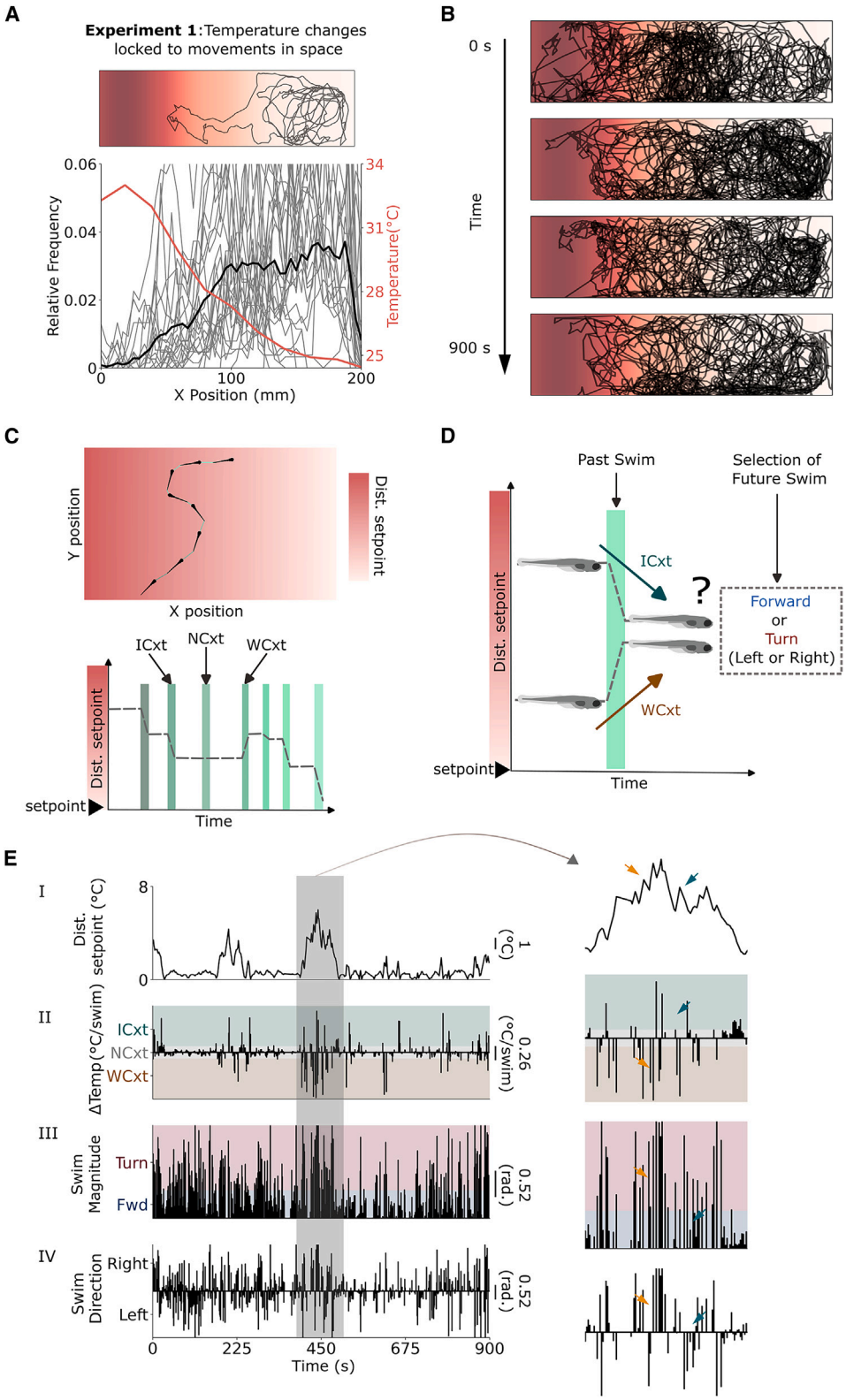

Figure 1. Larval zebrafish maintain homeostasis in a linear shallow thermal gradient

(A) Top: example trajectories of three fish for the entire duration of the experiment (15 min). Actual temperature measured in the water is pictured with different shades of red. The highest temperature (33°C) is represented on the left by the dark red. Bottom: histogram of animals' x-position in the arena (n = 26, gray traces), median of the population (black trace) and temperature measurement (red trace).

(legend continued on next page)

Using a combination of whole-brain calcium imaging, circuit perturbations, and behavioral phenotyping, we identified two evolutionary conserved brain structures, the PoA and the dorsal habenula (dHb), a homolog of mammalian medial habenula (Hb), as critical players for homeostatic navigation. On one hand, PoA ablation impaired the increase in non-directional turning probability when temperatures worsened, which is the main drive behind all the relevant behavioral responses to a thermal gradient. By contrast, dHb-ablated fish retained the drive to reorient when sensory conditions were worsening but showed a selective impairment to move in a coherent direction away from unfavorable temperatures. Furthermore, we find that neurons in a small region of the right dHb respond to both thermal and salinity changes with similar dynamics. Thus, these neurons might convey multimodal input to downstream structures and have a modality-independent role in homeostatic navigation.

Based on our experimental data, we propose a model where the PoA and dHb are both involved in homeostatic navigation and support larval zebrafish thermoregulation. The PoA is necessary for detecting homeostatic stress triggering reorientation and relocation behavior, while the dHb couples the memory of the sensory experience to previous motor choices to drive coherent movement trajectories toward the preferred temperature. Finally, the dHb-IPN pathway also appears to be a generalist circuit for a more abstract representation of environmental context supporting homeostatic navigation.

RESULTS

Zebrafish perform homeostatic navigation by modulating the reorientation probability and direction

We first asked whether larval zebrafish, when placed in an arena with a shallow temperature gradient and in the absence of any other sensory cues, could navigate and stay close to a particular temperature or whether they would distribute themselves uniformly in the chamber. To this end, we designed a 20 cm × 4 cm rectangular arena (Figure S1A), where we selectively heated up a 4 cm × 4 cm area at one end to 33°C while keeping the other end of the arena at 24°C, effectively establishing a linear thermal gradient (see STAR Methods and Figure S1B) of 0.04°C/mm along the long side of the arena (Figure S1C). In this environment, the temperature difference across the length of the fish's body was at most 0.2°C. We monitored individual 5–7 days post-fertilization (dpf) zebrafish for 15 min (see STAR Methods) and found that by the end of the experiment, fish robustly avoided the hot side of the arena (Figure 1A). Given the x-coordinate of the fish within the arena, we could identify the temperature it experienced (using the red curve in Figure 1A, see STAR Methods). We observed that, after an initial exploratory phase of approximately 260 s, fish rapidly appear to prefer a temperature of ~25.3°C, which we posit to be their homeostatic setpoint (Figures 1B and S1D–S1F).

The difference between the currently experienced and the animal's preferred temperature is the fundamental drive for homeostatic navigation. This scalar quantity alone cannot, however, provide a salient directional cue that could instruct directed behavior,[11,12] which is required for the spatial relocation observed in our experiments. We reasoned that, similarly to chemotaxis, phototaxis, and rheotaxis,[13–16] the simplest directional cue is given by the temporal changes in temperature due to the animal's self-relocation[3,17] (Figure 1C). In this scenario, previously experienced temperatures could contextualize the current one and provide a basic notion of a worsening or improving context, driving either a change in or continuation of current behavioral output, respectively, such as increased turning versus forward movements, independent of the absolute temperature.[17] A worsening context should increase the reorientation probability to change the fish's direction of traveling. On the other hand, an improving context, meaning getting closer to the homeostatic setpoint, should result in turning suppression in order to keep the current direction[3,12,13,17,18] (Figure 1D). Because larval zebrafish swim in discrete bouts, lasting ~300 ms and elicited at an approximate rate of 1 Hz,[19] context evaluation is likely to happen at the end of each swim event, as previously described for rheotaxis.[16] Experimental classification of swim bouts into forward swims and turns is easy because these are known to be kinematically very different.[19,20]

By taking into account the temperature change experienced by the fish during the last motor action (see STAR Methods), we were able to define three scenarios. An improving context (ICxt) when the temperature change was toward the fish's setpoint independent of the absolute temperature experienced, a worsening context (WCxt) when the fish moved away from the setpoint and no context (NCxt) for an isothermal movement. Figure 1E shows an example fish moving in the arena together with all the relevant stimulus and behavioral variables we extracted from the trajectory. In the close up of a behavioral sequence (Figure 1E right), we analyzed several periods where the animal experienced the same temperature but in two different contexts (orange arrow for WCxt and blue arrow for ICxt). In the WCxt (orange arrow) the reorientation probability is highly modulated and the turning frequency increases. Moreover, as shown in the bottom panel, fish tend to concatenate turns in the same direction, such that a right turn is subsequently followed by right turns and

(B) Trajectories of all the fish split in 3-min bins.
(C) Top: sketch of an example trajectory. Bottom: change of temperature perceived over time for each swim event in the top sketch. Time is coded by the shades of green (from dark to light green). Arrows on top point to a movement in a ICxt (improving context), NCxt (no context), and a WCxt (worsening context), respectively.
(D) Sketch of information available to the fish for behavioral choice using the sensory context provided by the previous swim.
(E) Summary of all the stimulus and behavioral variables used in this study for a representative individual fish. On the left: the entire duration of the experiment. On the right: close up of the trajectory and the relevant variables highlighted in the gray box. The four graphs show: (i) temperature experienced by an example fish, (ii) ΔTemperature (difference in temperature between current and last movement) experienced (color coding represents: worsening of conditions [in brown, away from physiological setpoint], improvement [in turquoise, toward physiological setpoint], or no change [in gray]), (iii) the absolute value of reorientation for each swim (color coding represents: turn [in red, when reorientation is higher than 30°], or forward [in blue, when reorientation is lower than 30°]), and (iv) the direction of turns, either left or right.
See also Figure S1.

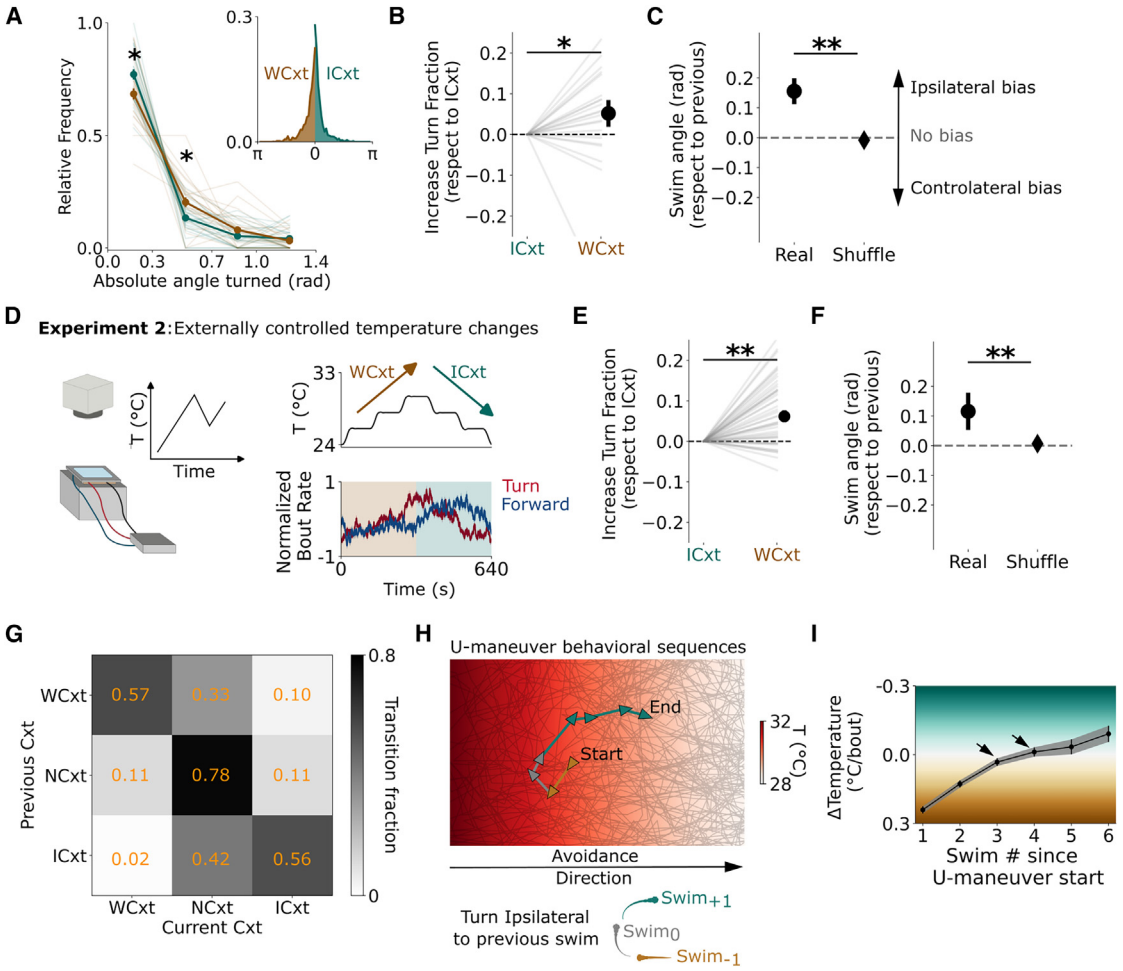

Figure 2. Homeostatic navigation is performed by combining an adirectional with a directional strategy

(A) Relative distribution of the absolute angle turned when fish experienced a WCxt or an ICxt (mean ± standard error of the mean, Mann-Whitney nonparametric test with Bonferroni correction for multiple comparisons).

(B) Normalized increase in turn fraction depending on sensory context (median ± standard error of the median, Mann-Whitney nonparametric test).

(C) Direction of swim during WCxt according to the direction of the previous swim (mean ± standard error of the mean, Mann-Whitney nonparametric test). Positive values imply that the swim tends to be in the same direction as the previous one. Diamond on the right is a shuffle obtained by assigning the sign for each value randomly.

(D) Left: behavioral setup. Right top: stimulus protocol for temporal gradient experiment. Right bottom: average normalized turning rate (red) and forward-swim rate (blue) for n = 40 fish.

(E) Increase in turning fraction depending on sensory context for experiment 2, similar to (B) (median ± standard error of the median, Mann-Whitney nonparametric test).

(F) Turn correlation upon WCxt for experiment 2, similar to (C) (mean ± standard error of the mean, Mann-Whitney nonparametric test).

(G) Mean transition matrix for sensory context across fish population.

(H) Top: example U-maneuver performed during experiment 1. Bottom: sketch of a U-maneuver.

(I) Difference in temperature experienced by fish during the execution of U-maneuvers, starting from in a WCxt (mean ± standard error of the mean).

See also Figures S2 and S3.

vice versa. In this way, each swim event of a larva could be assigned a behavioral category corresponding to left turn, right turn or forward swim, and a context change WCxt, ICxt, or NCxt, depending on whether the swim event took the fish further away from the physiological setpoint, brought it closer to it, or had no effect.

By plotting the relative distribution of the absolute angle turned for all fish for WCxt and ICxt (Figure 2A), we confirmed our previous observation that temperature context influences reorientation. Worsening of experienced temperature led to higher probability of reorientation. This difference in the distribution of turn angles was absent within a control group in which fish were permitted to swim within the arena without the presence of a thermal gradient (see Figure S2A, see STAR Methods). For simplicity, we also generated an index that allowed us to quantify the amount of reorientation driven by sensory context in future analysis. Specifically, we computed the difference between the turn fraction during WCxt and the turn fraction during ICxt. Again, this index exhibited a

significant difference (Figure 2B). Notably, when we repeated similar analyses on other swim kinematic parameters such as distance traveled (Figure S2B), swim duration (Figure S2C), and interswim (interbout) interval (Figure S2D), no significant context-dependent modulation was observed. Moreover, we noticed that the direction of turning was not stochastically decided during each movement.[21] In fact, when we quantified swim direction with respect to the previous turn event in the WCxt scenario, we found a high correlation, suggesting a form of memory used by the fish to persist in the previously chosen direction (Figure 2C).[21] Although this correlation was already observable in the absence of a thermal gradient and under both ICxt and NCxt conditions, its magnitude was increased in the WCxt condition (Figure S2E). These data indicate that fish not only turn more when the conditions worsen (WCxt, i.e., non-directional strategy) but that they perform sequences of turns in the same direction (i.e., directional strategy).

In order to test the robustness of the increase in reorientation probability and directional persistence across different time scales, we challenged the fish in another set of experiments with a step-like ramp ranging from 24°C to 30°C. Specifically, every 2 min, the temperature changed in the whole arena by 2°C (Figure 2D, see STAR Methods). For these experiments, we used a square-shaped, smaller arena, which allowed the temperature to change homogeneously throughout (Figure 2D left). The fish was, just as before, able to swim freely. Just as in the previous experiment, analysis of the turn fraction (Figures 2D, 2E, S3A, and S3B, see STAR Methods) showed that turns were indeed upregulated by sensory context producing more reorientation maneuvers when the temperature was moving away from the preferred setpoint. Furthermore, analysis of consecutive turns in the WCxt epoch confirmed also the high temporal correlation of turning direction (Figure 2F),[21] which was diminished during ICxt (Figure S3C). This result highlights both the robustness and replicability of the fish's behavioral strategy across different setups and conditions and the finding that temporal structure alone can induce these changes in strategy.

Unlike the previous experiment, here, the sensory context remained relatively constant for an extended duration, and the fish had no control over the temperature experienced, as the temperature changed every 2 min. Consequently, the time elapsed between two swim events where the fish experienced a change of temperature could be significantly longer than in the spatial gradient experiment. We investigated whether this feature influenced the previously described correlation in turning direction during WCxt. We hypothesized that, the more time elapsed between two turns and their sensory consequences, the less likely it would be for the direction of these turns to be correlated. When we repeated the same analysis described above, but now considering the interswim interval between the two turns, we confirmed this hypothesis (Figures S3D left and S3D right for the average number of events considered in each temporal bin).

In the large rectangular arena, we noticed, that due to the shape of the temperature gradient (Figures S1B and S1C), it was improbable for the fish to move from a WCxt to an ICxt in a single swim, as shown by the overall distribution of difference in temperature experienced during swims (Figure S3E) and the transition matrix between sensory contexts (Figure 2G). Such context transitions usually take several swim events, where many of those movements do not provide any useful information about the change in temperature (NCxt). We hypothesized that fish could nevertheless use past changes in temperature and combine them with previous motor choices to persist in their behavioral program. We confirmed that fish were prone to reorient more when coming from a WCxt even if they did not experience a change in temperature during their last movement (NCxt) (Figures S3F and S3G). This observation does not depend on the threshold used to define NCxt and is therefore unlikely to arise from an analysis artifact (Figure S3H). In fact, the reorientation sequences produced U-shaped trajectories (U-maneuvers) commonly ending with the fish facing in the opposite direction to where it started from, toward the preferred temperature (Figure 2H). In order to quantify these observations, we extracted all the U-maneuvers started in a WCxt and computed the average temperature difference experienced by the animals during the execution of these behavioral sequences (see STAR Methods). In line with our previous observations, directional swims persisted in the direction defined during WCxt even in the absence of new sensory cues (Figure 2I, see swims 3 and 4 indicated by the black arrows).

To summarize our behavioral observations (Figures 1 and 2), we found that larval zebrafish perform homeostatic navigation by modulating the reorientation probability depending on the sensory context experienced while swimming. Going away from the homeostatic setpoint elicits increased turning. Moreover, the direction of such reorientation maneuvers tends to be coherent, as in the observed U-maneuvers. We finally observed that these maneuvers persist even in the absence of immediate sensory directional cues (NCxt) and can therefore be interpreted as the fish being in a motor state and implementing a directional strategy.

A whole-brain functional screen identifies brain regions modulated by sensory context

Our behavioral experiments indicate that zebrafish larvae regulate body temperature by making use of both a sensory context and history and a motor-dependent behavioral strategy. We then took advantage of the optical transparency of larval zebrafish to perform a whole-brain functional screen using lightsheet microscopy. We used transgenic animals expressing a nuclear localized GCaMP6s in most of the neurons (n = 5, 6–8 dpf, *Tg(elavl3:H2B-GCaMP6s)*, Video S1) to identify brain regions responsive to temperature, putatively involved in homeostatic navigation.

To control the temperature experienced by the fish while embedded and during imaging, we placed a small needle close to the fish's head. This provided a constant flow of water through a multivalve system, which could also be heated or cooled down upstream of the tube by a Peltier element (see STAR Methods, Figure 3A). A high-speed camera was used to track the behavioral tail movements of the larva while it was being imaged. We first delivered the same stimulus protocol as in Figure 2D (Figure 3A top right) and in a small subset of fish (n = 2) we performed lightsheet whole-brain imaging. Behaviorally, we again observed a modulation of the reorientation probability depending on sensory context and direction for WCxt, replicating our freely swimming data (Figure 3A bottom right, Figures S4A–S4E). When we extracted neurons that reliably responded to the three trials (see

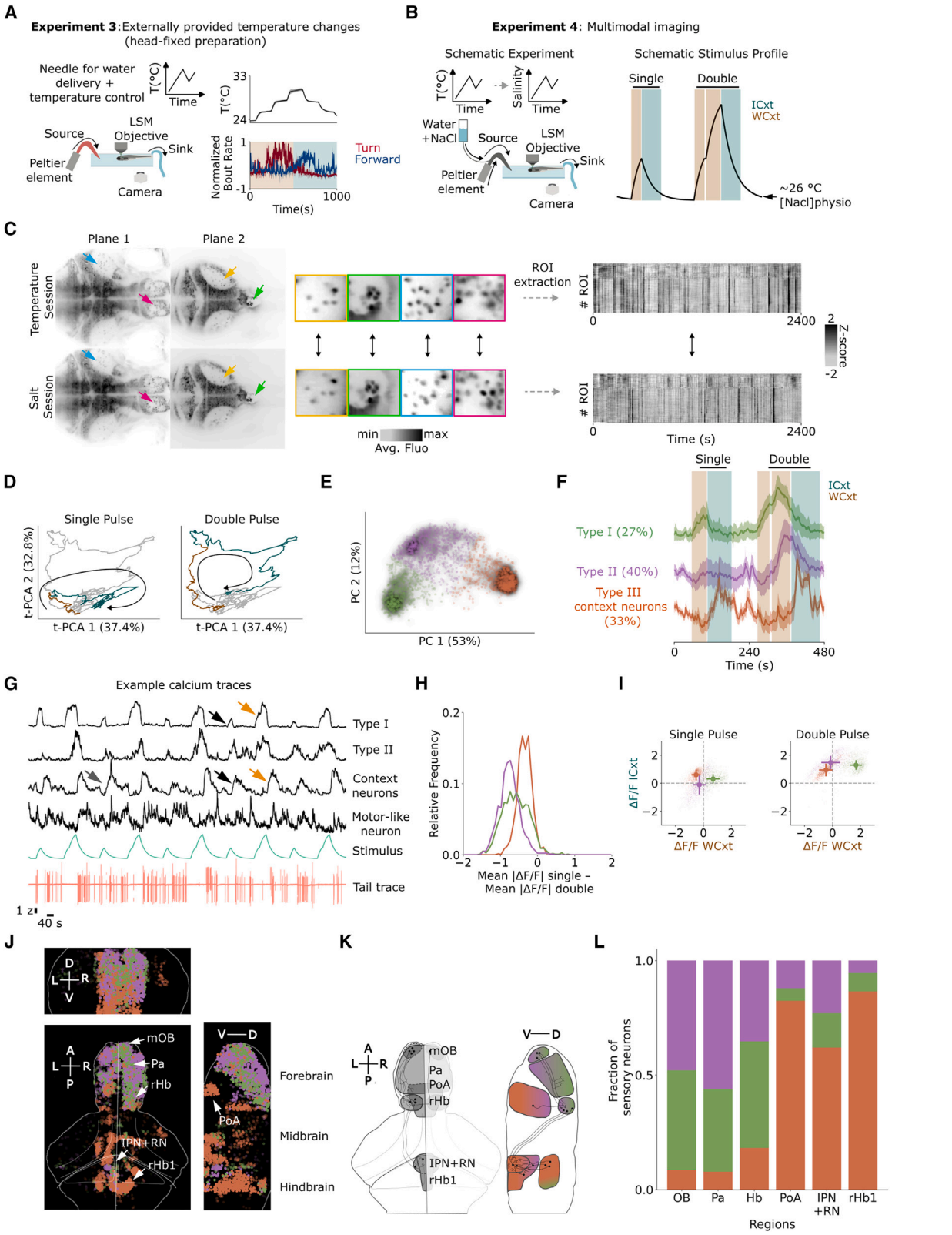

Figure 3. Identification of neurons encoding sensory context in a whole-brain screen

(A) Left: schematic representation of the head-restrained preparation for the lightsheet setup. Top right: protocol as in Figure 2D. Bottom right: average normalized turning rate (red) and forward-swim rate (blue) for n = 11 fish (mean ± standard error of the mean).

(legend continued on next page)

STAR Methods), we observed responses in multiple regions, such as the olfactory bulb (OB), pallium (Pa), right habenula (rHb), preoptic area (PoA), interpeduncular nucleus (IPN), and superior raphe nucleus (RN) (Figure S3H).

Although this protocol elicited a strong and clear behavioral modulation, the relatively long duration of each trial (~20 min) was not optimal for an imaging experiment, where more repetitions are beneficial. Moreover, in this assay, the observed neuronal responses could be due to either temperature sensing or motor behavior: given the strong correlation between the stimulus protocol (upward vs. downward temperature gradient) and the animal's behavior (turn vs. forward). We therefore devised a protocol with five repetitions of a shorter stimulus block. In each block, fish experienced an increase of +0.25°C away from their preferred temperature (~ 26°C) before the temperature was brought back to baseline (single pulse). Then the increase was repeated, but this time the temperature was subsequently further increased to ~26.5°C (double pulse) (Figures 3B and 3B right). The rationale behind this protocol is to present the fish with a situation that can either improve after getting worse (single pulse, ICxt) or get worse again (double pulse, WCxt), thus mimicking the naturally occurring scenario that the fish encounters while swimming freely. We proceeded to use this protocol to acquire our main whole-brain dataset.

Temperature is not the only environmental factor that poses a homeostatic threat and leads to an asymmetric behavior when the animal is pushed away from its homeostatic setpoint.[12] We asked whether the fish brain encodes a representation of stimulus history that generalizes across different sensory modalities, regardless of the stimulus identity. We therefore recorded brain activity during transient increases in salinity (salt session), which can be equally threatening to the animal's physiology.[12,22] Importantly, we were able to qualitatively match the stimulus profile of the salt session with the temperature session (Figures S4F and S4G, see STAR Methods) to properly compare brain responses. In addition, we matched single neuron identity across the two sessions (Figure 3C, see STAR Methods) and extracted their fluorescence throughout (see a subset of ROIs activity for an example fish in Figure 3C right). For each fish (n = 5), we extracted 44,772 ± 7,090 (mean ± SD) ROIs, likely corresponding to single neurons, spanning the forebrain, midbrain, and parts of the hindbrain up to rhombomere II.

We first focused our analysis on the temperature session. For each neuron, we computed the average correlation across the five trials (reliability index) and used the trial-triggered average responses (TTA) to find consistent TTAs across individuals (see Figure S3G and STAR Methods). This approach aimed to identify neurons that consistently responded to temperature stimulation and shared their responses across fish. We selected only "reliable neurons" using a fixed standard threshold criterion for all. We then employed an unsupervised approach (principal component analysis [PCA]) to reduce the dimensionality across the time dimension, with the goal of investigating which stimulus characteristics were mostly influencing neural activity. When looking at the first two PCs (cumulative variance explained 70.2%, Figure 3D), we observed that the population trajectory appeared to separate WCxt and ICxt along the t-PC1, but also the stimulus intensity along the t-PC2. To better understand what type of neuronal responses were responsible for the context-dependent activity, we performed PCA in the other dimension so that each dot in the space defined by the first two principal components shown in Figure 3E represents the average single neuron response during stimulus presentation (cumulative variance explained 65%, Figure S5A). Since 3 clusters were clearly observable, we performed k-means clustering (k = 3) using the coordinates in the PC space in order to describe common neuronal responses. The number of clusters was further checked using the Davies-Bouldin score (see STAR Methods and Figure S5B).

The three clusters corresponded to three populations of neurons: a population following the stimulus profile (type I), a population showing an increase in activity upon temperature rises with a longer rise constant (type II), and a population that showed a reduction in baseline fluorescence when temperature increased (WCxt) and an increase in fluorescence when temperature decreased (ICxt) (type III) (Figure 3F). As shown by the raw traces in Figure 3G, the sensory responses do not arise from an averaging artifact or motor activity. They are already visible within individual fish at the single trial level and are dissociated from purely motor-related activity. This observation was further quantified by comparing the correlation with motor activity between sensory neurons and putative motor neurons (Figures S5C and S5D). Neurons of type III are well suited to inform the fish on whether the temperature context is worsening or improving (context neurons). Moreover, when we computed the difference in average ΔF/F

(B) Left: schematic representation of the multimodal experiment. Right: short protocol used for the lightsheet imaging experiments.
(C) From left to right: anatomy of an example fish during the temperature and salt sessions. Yellow, green, cyan, and purple arrows indicate four different patterns of neurons visible in both sessions. Raw activity of 10% of neurons (randomly selected) in a dataset for both temperature and salt session. Arrangement of the traces has been done according to the rostro-caudal position of selected ROIs.
(D) Temporal trajectories in PC space of the neuronal activity of reliable neurons, color-coded based on stimulus context (brown WCxt and turquoise ICxt).
(E) Projection onto PC space of all reliable neurons color-coded according to their cluster identity.
(F) Mean activity of each cluster (mean ± standard error of mean) and fraction of cells per group (tot n = 3,270).
(G) Example raw traces from the three clusters and one motor ROI (all in black), the approximate stimulus profile (green) and the tail trace showing behavior (pink).
(H) Relative frequency distribution of the difference in mean fluorescence change during the single and double pulse stimulation for each cluster. Negative values imply that the fluorescence increased with increasing absolute temperature.
(I) Scatter plot of the average deviation from baseline fluorescence during single (on the left) and double pulse (on the right) split by sensory context (WCxt and ICxt) for the neurons in the three clusters (mean ± standard error of mean).
(J) Left: anatomical distribution of reliable ROIs according to cluster identity. Different panels depict different projections. mOB, medial olfactory bulb; Pa, pallium; rHb, right habenula; PoA, preoptic area; IPN + RN, interpeduncular nucleus and raphe nucleus; rHb1, rhombomere 1. Right: sketch of hypothesized synaptic connections based on activity maps and literature.
(K and L) Proportion of ROIs from the different clusters for different anatomical regions. OB, olfactory bulb; Pa (Pallium); Hb, habenula (left + right habenula); PoA, preoptic area; IPN + RN (interpeduncular nucleus + superior raphe nucleus), rHb1 (rhombomere 1).
See also Figure S4.

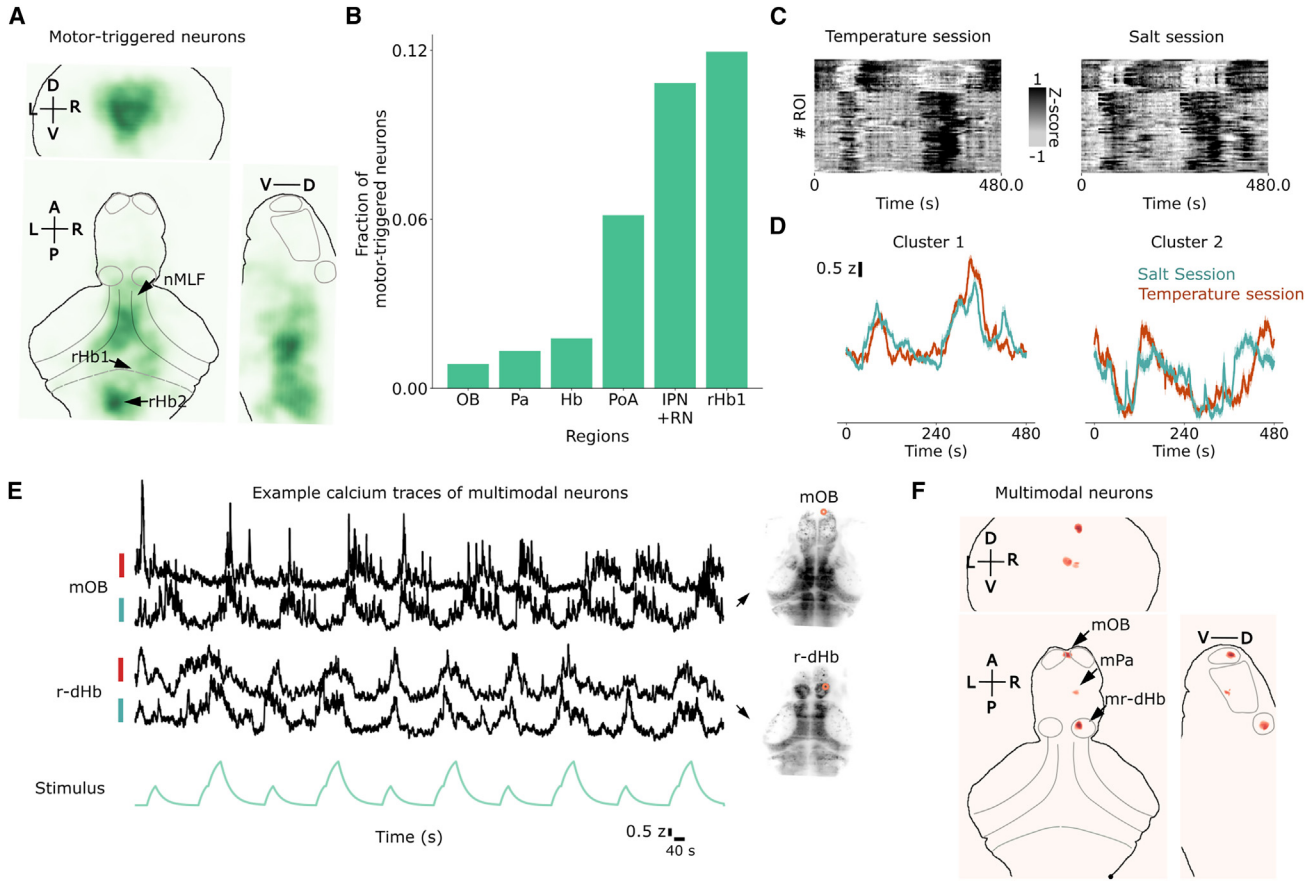

Figure 4. A small population of dorsal habenula, medial olfactory bulb, and pallial neurons respond similarly to temperature and salinity changes

(A) Anatomical density distribution of motor-triggered ROIs. Selected cells can be either forward, left, or right-swim tuned.

(B) Fraction of motor-triggered ROIs for each sensory-identified region.

(C) Trial trigger average of all multimodal neurons found during temperature (left) and salt (right) sessions.

(D) Mean of the multimodal neuron clusters (k = 2, mean ± standard error of the mean).

(E) Raw activity of two example multimodal neurons (one from the olfactory bulb and one from the habenula) in black for both the temperature and the salt session.

(F) Anatomical density distribution of multimodal neurons for the three projections. mOB, medial olfactory bulb; mPa, medial pallium; mr-dHb, medial nucleus of the right dorsal habenula.

See also Figure S5.

between the single and the double pulse within the stimulus block, we found that activity in type I and type II neurons were modulated by absolute change in temperature. On the other hand, activity in context neurons showed minor modulation, suggesting that responses in this cluster did not scale with stimulus intensity (Figure 3H, see also raw traces in Figure 3G, black and orange arrows). Finally, we decided to plot the ΔF/F during WCxt and ICxt, as defined in Figure 3B right, either during the single (Figure 3I, left) and double pulse (Figure 3I, right) periods. In this plot, if neurons are localized in the first and third quadrant, they respond congruently across contexts, whereas if neurons are localized in the second or fourth quadrant they show an asymmetric response. In our case, type I neurons were localized in the first quadrant with an increase in ΔF/F during the double pulse, suggesting a coding for stimulus intensity and a symmetric response to context. Type II showed non-linear responses for the two pulses. Finally, type III neurons were localized in the second quadrant, and they did not show a modulation in ΔF/F between the single and double pulse, suggesting a coding for sensory context with a reduction from baseline fluorescence during WCxt and an increase during ICxt.

Importantly, when we looked at the anatomical distribution of the three clusters (Figure 3J, left) we noticed that type I and II neurons were enriched in rostral regions, such as the medial olfactory bulb (mOB), Pa, and rHb, whereas context neurons were found in other regions such as the PoA, anterior hindbrain (aHb), IPN, and RN. Most of the aforementioned regions are known to be strongly connected (Figure 3K).[23–28] In fact, we observed a functional gradient along the mOB-Pa-Hb-IPN-RN pathway, with upstream regions mostly responding to absolute temperature and downstream regions, together with the PoA, mostly tracking the stimulus context (Figure 3L).

Having identified several brain regions enriched in context neurons, we next wanted to find putative pre-motor areas that could use this information to influence behavior. Therefore, we searched for cells that were reliably activated by either forward, left, or right swims (Figures 4A and S5E and STAR Methods). In line with other

reports,[29–33] we observed neural correlates of motor activity around the nucleus of the medial longitudinal fasciculus (nMLF) and hindbrain regions. We also examined the localization of motor-related signals in brain regions that were previously identified as crucial for tracking stimulus features (the neurons of types I, II, and III). We noticed that regions with a higher number of context neurons tended to also have more motor correlates (Figure 4B), although in a different population respect to sensory neurons (Figure S5C).

Finally, we looked for multimodal neurons with similar stimulus-response profiles for both the salt and the temperature sessions. We cross-correlated the TTAs of reliable neurons in both sessions and then computed a p value based on circular shift shuffle versions of such traces (see STAR Methods). We selected neurons with p value < 0.025 (Figures 4C and S5F) and clustered them into two groups for visualization purposes (Figure 4D). This analysis revealed neurons with similar dynamics upon temperature and salinity changes (Figure 4E). Although all the previously identified sensory regions had neurons responding during both sessions (Figure S5G), only the medial nucleus of the right dHb (mr-Hb), the mOB, and a small region in the Pa had multimodal neurons (Figure 4F).

In summary, our whole-brain analysis confirmed that temperature is sensed by neurons located in the olfactory system,[7] probably among other regions that were not imaged in this study, such as the trigeminal ganglion.[34] This information is then broadcast to hypothalamic regions, such as the PoA and to the dHb-IPN-RN system. The PoA was particularly enriched in temperature-specific context cells,[22] which suggests a role in thermoregulation (i.e., as a thermostat), just as in mammals.[7,35–39] Regarding the dHb-IPN-RN system, the situation is more complex. Although responses in the dHb are mainly sensory, responses in the IPN, the main target of the dHb, were enriched in context and motor-modulated cells. The Hb is also known to receive direct input from the OB through the Pa and minor inputs from the PoA.[26,28] Finally, the Hb was also particularly enriched with neurons that generalized across modalities.[40,41] Overall, our imaging results suggest that both the PoA and the Hb are involved in homeostatic navigation.

PoA and dorsal habenula ablations impair different aspects of homeostatic navigation

In our whole-brain functional screen, we identified the PoA and the dHb-IPN-RN system as candidate pathways to provide information about the stimulus context. Considering the role of the PoA in thermoregulation in mammals and the involvement of the Hb in other sensory-driven navigation assays in larval zebrafish, we hypothesized that they could both be involved in homeostatic navigation. To test this, we ablated the PoA or the dHb and analyzed the behavior of the fish in the spatial gradient arena.

Bilateral ablations of the PoA (n = 20 fish), as functionally identified in our previous lightsheet experiments, were performed with a Ti-Sapphire laser at 5 dpf (Figures 5A and S6A). As a control, we targeted part of the medial optic tectum (OT) because this region was poorly activated by temperature stimuli (n = 20 fish, see STAR Methods). After the ablation procedure, fish were left to recover for 40–48 h and tested at 7 dpf. Ablation of the PoA produced a higher coefficient of dispersion in the thermal gradient at the end of the experiment compared with controls, suggesting an impairment in staying near their homeostatic setpoint (Figures S6B and S6C, see STAR Methods). To test this hypothesis, we computed the same increase in turn fraction as we did for wild-type fish in Figure 2B. Following the PoA ablation protocol, fish showed a significant impairment in the modulation of reorientation probability depending on sensory history (ICxt vs. WCxt) with respect to controls (Figure 5B). The absence of such modulation is also reflected in the reduction of turn fraction, compared with controls, during the entire experiment (Figure S6D) but no general motor impairment was observed, as shown by the fish swims rate (Figure S6E). Notably, also the directional persistence to change orientation through U-maneuvers when the fish experienced a WCxt was impaired (Figure 5C). These results suggest that the PoA is involved in driving the turning behavior observed in homeostatic navigation.

We next used the transgenic *Tg(Gal4:16715; UAS:Ntr-mCherry)* line to ablate the dHb at 5 dpf using a chemogenetic approach (see STAR Methods). This line restricts the expression of nitroreductase to the dHb (Figures 5D, S6F, and S6G). As control groups, we used a genetic control and a treatment control (n = 25, 23, and 14 for genetic control, treatment control, and ablation group, respectively). In contrast to the PoA ablations, although the group dispersion coefficient was higher for dHb-ablated fish compared with controls (Figure S6I), dHb-ablated fish were still able to modulate their reorientation probability based on sensory context (Figure 5E). However, when we tested whether sensory history before the last immediate action would introduce a bias in turning direction, we observed that the correlation in swim direction (underlying U-maneuvers) was impaired in Hb ablated fish compared with controls (Figure 5F). Moreover, when the fish had access to intermittent sensory cues (e.g., WCxt → NCxt or ICxt → NCxt), the increase in reorientation probability in the WCxt was lost in the ablated group (Figure S6J). Finally, we observed a general upregulation of reorientation maneuvers in the ablated group (Figure S6K) but no significant change in swim rate compared with controls (Figure S6L).

These results confirm our findings from the calcium imaging experiments and reveal that the PoA and the dHb are both involved in homeostatic navigation, and they jointly support it.

To summarize, we have shown that the PoA supports homeostatic navigation and, specifically, thermoregulation by driving reorientation maneuvers upon worsening of conditions.

On the other hand, the Hb seems to impact mainly the generation of coherent steering trajectories, which could help the animal in localizing its preferred temperature in shallow temperature gradients where individual movements do not always bring a change in environmental conditions. Thus, the dHb supports the fish in directional navigation in the absence of constant new information after each movement.

DISCUSSION

In this study, we have shown that the larval zebrafish, an ectotherm, can navigate a shallow thermal gradient to locate its preferred environmental temperature and thereby achieve temperature homeostasis. This contrasts with endotherms such as mammals who rely on autonomic responses in addition to behavioral adjustments.[6] Importantly, our data reveal that temperature homeostasis in an ectotherm still relies on the PoA,

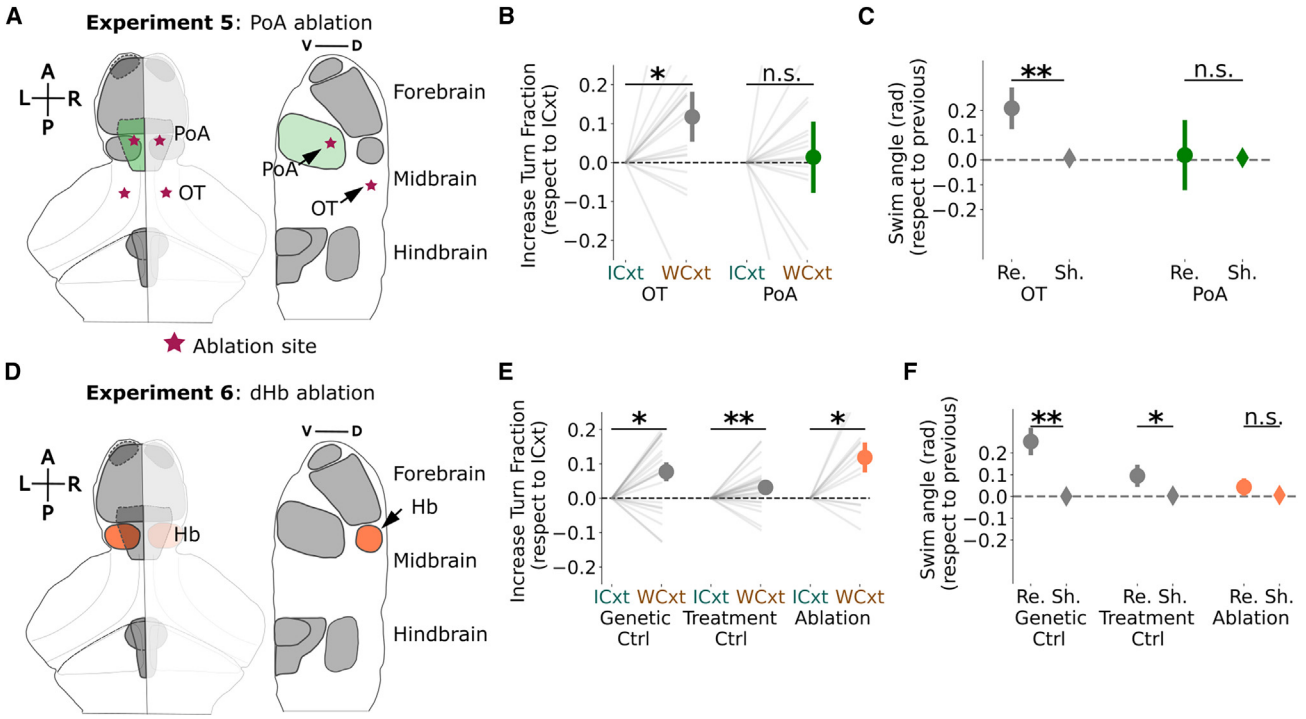

Figure 5. PoA and dorsal Hb ablations impair different aspects of homeostatic navigation

(A) Sketch of 2-photon ablations targeting the PoA (depicted in green). Stars are the chosen ablation sites. The control ablation is in the optic tectum (OT) (see text).

(B) Increase in turn fraction depending on sensory context. Left: control OT ablation, right: PoA ablation. (median ± standard error of the median, Mann-Whitney nonparametric test.)

(C) Turn correlation upon WCxt for the control and ablation groups (mean ± standard error of the mean, Mann-Whitney nonparametric test).

(D) Sketch of chemogenetic ablations targeting the dHb (depicted in orange).

(E) Increase in turn fraction depending on sensory context. Left: genetic control, middle: treatment control, right: dHb ablation (median ± standard error of the median, Mann-Whitney nonparametric test).

(F) Turn correlation upon WCxt for the two controls and the ablation group (mean ± standard error of the mean, Mann-Whitney nonparametric test).

See also Figure S6.

the internal thermostat of the mammalian brain. Moreover, our results suggest that the dHb, enables precise temperature homeostasis in environments with slow or minor temperature changes through a simple working memory.

More specifically, the strategy larval zebrafish use involves comparing the temperature before and after a swimming event and biasing their subsequent action based on whether the new temperature approached their preferred setpoint (ICxt) or was further away from it (WCxt). In the first case, the fish responds with more forward movements, while in the latter case, they reorient in order to change their direction of travel (Figure 6A, left). This non-directional strategy is widely used across the animal kingdom when navigating many different sensory gradients[3,12–16,18,42,43] and has been referred to as behavioral hysteresis.[17]

Interestingly, the probability of a type or category of swim (turn vs. forward swim) was the only behavioral parameter modulated by the context (WCxt or ICxt). Kinematic parameters of the swim categories such as swim distance, swim duration, and inter-swim interval are only influenced by absolute temperature.[11] Based on this evidence, we suggest that apart from the swim category, all the other behavioral changes most likely reflect a stress-like state triggered by an unescapable homeostatic threat, rather than a navigation strategy. This idea is further supported by the fact that although the modulation of turn fraction, swim distance, swim duration and directional coherence scales linearly with an increase in absolute temperature, fish still avoid cold temperatures and localize their homeostatic setpoint by upregulating their reorientation maneuvers when moving away from their preferred temperature.[44] Therefore, we posit that behavioral hysteresis is the main building block in homeostatic navigation.

In our experiments, we also observed that fish tend to concatenate reorientation events, where a turn is likely followed by another one in the same direction.[45] Again, this observation contrasts with the effect of the absolute temperature where directional coherence is strongly reduced at high temperatures.[11] Finally, we found that, when a swim led to neither an improvement (ICxt) nor worsening (WCxt), fish were still able to leverage their memory of the sensory history before the last movement and combine it with the knowledge of the previous movement direction to generate coherent U-maneuvers (Figure 6A, right).

We find it intriguing that similar sensorimotor strategies have also been described in different types of temporal and spatial taxis assays.[12,16,46,47] This suggests that fish can also have an abstract representation of context, independent of the sensory

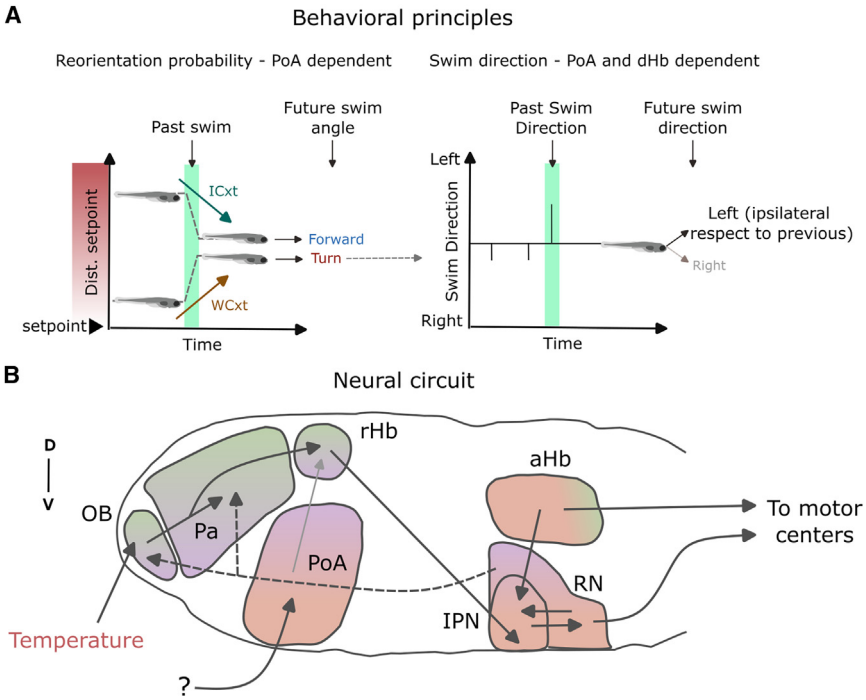

Figure 6. Homeostatic navigation

(A) Behavioral principles underlying homeostatic navigation in larval zebrafish uncovered by this study. Fish use two complementary strategies: an increase in turning (reorientation probability) when experiencing a WCxt (being pushed away from the homeostatic setpoint, left panel) coupled with turning in a persistent direction during this WCxt (right panel). The first strategy is PoA dependent, whereas the second depends on both the PoA and the dorsal Hb.

(B) Neural circuitry involved in homeostatic navigation. Neurons representing the three main different stimulus features are represented in different colors and the anatomical shading shows the fraction of response types in each region.

modality. Indeed, we found individual neurons that convey context independent of the sensory modality. Fish could then use a unique navigational system informed by different sensory modalities via the context, rather than independent parallel unimodal circuits.

Overall, our behavioral data show that homeostatic navigation is more complex than a simple reflexive stimulus-response behavior, although physiological stress still represents its main trigger.[22,48,49] The behavioral mechanisms involved in this process go beyond the moment-by-moment estimate of the sensory input with respect to the homeostatic setpoint. We propose that even when new sensory information is absent, fish can still use their past motor choices to guide an internally generated motor program. This program has a directional component and impacts several subsequent swimming events. Thereby, fish can achieve precise temperature regulation also in slow or minimally changing temperature environments.

The neural circuit enabling homeostatic navigation

Taking advantage of whole-brain functional imaging, we identified brain regions responding to temperature changes in an open-loop virtual gradient assay (Figure 6B). Temperature responses predominantly fell into three functional types. Type I and type II neurons responded to the stimulus profile but with different dynamics, whereas type III tracked stimulus change (context neurons). The activity of context neurons was bidirectionally modulated, with a reduction from baseline during WCxt and increased activity during ICxt. Their activity was not influenced by stimulus intensity. We also observed a functional gradient along the rostro-caudal anatomical axis. Neurons of type I and II were mostly localized in the forebrain of the fish. The medial olfactory bulb (mOB) and the pallium (Pa) had almost exclusively type I and type II cells, whereas the right habenula (rHb) showed a mixture of type I, II, and context neurons. A possible interpretation as to why we see activity in regions traditionally linked to olfaction could be that, in a water medium, temperature and chemicals (such as odors) tend to have similar spatiotemporal statistics; therefore, it is advantageous to exploit the same sensory circuit for both. Interestingly, temperature sensing in olfactory circuits has also been found in other animals.[50–52] This interpretation is supported by reports of the recruitment in larval zebrafish olfactory regions upon exposure to salt,[12] changes in pH,[22] and carbon dioxide.[53]

On the other hand, context neurons were predominantly, with the notable exception of the preoptic area (PoA, see below), found in the fish midbrain and hindbrain in regions, such as the anterior hindbrain (aHb), the interpeduncular nucleus (IPN), and RN. Interestingly, bidirectional modulation of neuronal activity in rhombomere I has also been recently reported in an OMR-based decision-making paradigm involving leftward and rightward visual motion stimuli.[33] This commonality raises the possibility that neurons in these regions are not involved in sensory processing per se but in the selection of two opposite behavioral strategies based on sensory context.

Most of the regions mentioned above are also known to be strongly connected. Specifically, neurons in the mOB project to both the Pa and the rHb, often via collaterals of the same neuron.[26–28] Minor projections from the PoA[26] are also known to target the dHb. The Hb, then, sends glutamatergic input to the IPN through the fasciculus retroflexus.[23,24] In particular, neurons in the rHb selectively project to the ventral portion of the IPN with axons wrapping around this structure. Finally, the IPN is a GABAergic nucleus projecting to RN and receiving inputs from the aHB.[23,54] Strikingly, the RN sends axons to more caudal rhombomeres, as well as feedback projections back to forebrain regions, such as the OB and Pa.[55] We, therefore, suggest that these regions are part of a brain-wide network supporting homeostatic navigation.

Preoptic area—A homeostat in ectotherms?

We investigated a potential role of the PoA in larval zebrafish thermoregulation because this structure is critical in mammals

for maintaining a stable body temperature, it was previously linked in temperature perception and fever regulation[9,10] in ectotherms and, in our experiments, was particularly enriched in context neurons. Following the bilateral ablation of this region, we found a deficit in the test group in reaching thermal homeostasis. Fish failed to modulate their reorientation probability depending on the sensory context with respect to controls.

Unlike the dHb pathway (mOB-rHb-IPN-RN), less is known about PoA anatomy in larval zebrafish. Because the main targets of the OB are the rHb, Pa, posterior tuberculum, and the ventral nucleus of the ventral telencephalon,[25] it is unclear whether the PoA receives temperature information from the OB, Pa, or other structures, such as the terminal nerve,[24] trigeminal, or dorsal root ganglion.[34]

These results are consistent with the previously proposed role of the PoA in larval zebrafish in detecting temperature changes[34] and reacting to various types of physiological stressors.[22,48,49] However, our results expand those findings by suggesting a role of the PoA in thermoregulation by evaluating moment-by-moment the sensory history with respect to the homeostatic setpoint and in driving reorientation maneuvers. Given our findings, we propose that the PoA can either function as a trigger for reorientation behavior when the fish experiences a WCxt specifically in a thermal gradient or generally when it experiences a homeostatic threat.[22]

In conclusion, we propose that the PoA plays an evolutionary conserved function in regulating body temperature across vertebrates. We suggest that this function has adapted to the physiology and the nervous systems of different organisms. In mammals, which have both autonomic and volitional strategies to cope with thermal stress, the PoA integrates peripheral and central temperature information[6,56] to increase thermogenesis and physical activity.[39] Conversely, here, we provide evidence that the PoA in larval zebrafish directly triggers active navigation as a homeostatic control mechanism in an animal without autonomic homeostatic mechanisms.

Our findings fit within a broader framework, suggesting that the PoA and the hypothalamus, in general, can influence behavior at faster timescales than previously thought.[57–60] In the future, it would be interesting to understand if particular cell subtypes in the PoA are specifically involved in thermal navigation, similar to how it was shown for nocifensive behavior,[48] and to gain further insight into the interplay between the PoA and the Hb-IPN-RN pathway. For example, this study did not rule out whether context representation in dHb downstream structures is computed locally *de novo* or is inherited from the PoA. The latter could be implemented through the direct, although weak, monosynaptic connections from the PoA to the dorsal Hb[26] or through indirect mechanisms such as neuromodulation or polysynaptic connections.

Dorsal habenula—The directional component of homeostatic navigation

Except for the PoA, all other brain regions in our whole-brain screen that were enriched in context neurons, namely, the IPN and RN, are located in the midbrain-hindbrain boundary, are mono-synaptically connected to each other and receive inputs from the habenula (Hb).

In our imaging experiments, the medial nucleus of the right dorsal habenula (mr-dHb), together with a small region in the medial olfactory bulb (mOB) and in the medial pallium (mPa), responded reliably to both increases in temperature and salinity with similar response profiles. These results are in line with other reports highlighting the contribution of the dHb to other types of sensory-driven navigation behaviors.[12,40,47,53,61,62] We suggest that the dHb-IPN-RN pathway could provide a more general estimate of environmental context to mediate an appropriate behavioral response. In this scenario, different sensory modalities would converge onto a single navigation circuit to instruct a shared behavioral strategy.

Contrary to our expectations, dHb ablation did not impair modulation of reorientation probability based on sensory context (i.e., ICxt and WCxt). However, the coherence in turn direction during WCxt was abolished. Moreover, the experimental group showed a reduced reorientation probability in the presence of intermittent sensory cues. The absence of motor correlates in this structure and the directional impairment observed in freely swimming fish suggests that the dorsal Hb conveys multimodal sensory information to target structures that modulate the directional component of homeostatic navigation (left vs. right) on a timescale longer than a single movement. Importantly, our results do not show that dHb is involved in the selection of acute directional movements. In fact, we observed a behavioral impairment only when we looked at the relationship between consecutive directional movements with respect to a change in temperature. Considering these results, the dHb seems to be required for coordinating multiple directional movements in time with respect to a homeostatically relevant sensory context.

In fish, the dHb and vHb (ventral habenula) are the homologs of the medial and lateral habenula (MHb and LHb) in mammals.[63,64] The dHb conveys information coming from the limbic forebrain to the interpeduncular nucleus (IPN),[65] while the vHb is directly connected to the median raphe (MRN). The dHb can be further subdivided in a lateral and medial subregion (dHbL and dHbM, respectively). These two subnuclei differ in size with respect to the left and right hemisphere. dHbL is bigger than the dHbM on the left hemisphere, while the opposite is true for the right hemisphere. These two subnuclei differ also for their downstream structures. The dHbL project to the dorsal IPN (dIPN), while the dHbM project to the ventral IPN (vIPN). Additionally, the dIPN sends projections to the griseum centrale and dorsal tegmental area, both localized dorsally to the IPN nucleus. Finally, the vIPN project to the MRN. The fact that in the current study and in other reports has been shown that the right portion of the dorsal habenula (rHb) is responding to environmental threats suggests that these threats are sensed through the dHbM system, and the information further is elaborated by the vIPN and MRN. Considering that the vHb sends direct excitatory projections to the MRN and the dHbM sends second-order inhibitory projections through the vIPN, it is tempting to speculate that the two structures are not two separate systems but provide opposing drives to the serotonergic nucleus.[66,67]

Although we have a clear understanding of the gross anatomical organization of the dHb-IPN system in zebrafish, its contribution in guiding behavior still remains relatively elusive. In adults, it has been shown that dHbL and dHbM act in opposite fashion to regulate social conflict,[68] potentiation of the dHbL pathway promoted a winner-like behavior state, while potentiation of dHbM resulted in a passive loser state of the animal. This system has

also been linked to learning paradigms, at both juvenile and adult stage. At the juvenile stage, it has been shown that ablation of dHbL impaired reversal in a conditioned place avoidance task.[69] In adults, zebrafish with impaired dHbL failed in a learning task with a directional egocentric rule but not with a cued external rule such as color.[70] Furthermore, the inactivation of dHbL biased behavioral selection in a fear paradigm.[66] In larvae, the same pathway mediates odor attraction,[58,60] CO_2 and salt avoidance,[10,59] phototaxis,[44] and stress control in simple learning assay,[71] and it has also been proposed that the dHb is a multimodal trigger network associated to state transitions during foraging behavior.[63]

Previous studies interpreted the behavioral impairment following dHb ablation in taxis assays as a shift in stimulus preference[47,61,62] and concluded that this structure conveys information about the stimulus valence to a behavioral module. The seeming discrepancy between these conclusions and ours can be reconciled by the difference in the stimulus landscape used and the amount of contextual information available to the animal in the arena. Here, we complement this model and propose that, rather than absolute valence, the dHb is an essential component for the generation of contextual relative valence signal computed from the animal's recent past which, then, modulates directional choices. This mechanism is particularly useful if the sensory landscape presents areas with few contextual cues, such as isothermal regions in shallow or slow changing gradients or split field arenas.[47] The dHb's role in homeostatic navigation might be a functional precursor of more complex cognitive abilities observed for this region in adult zebrafish adult and mammals, such as valence[67] and direction-based decision-making[70] and strategy switching.[69,72]

In future work, it will be crucial to elucidate the, possibly, distinct roles of dHbL and dHbM because, in this study, both subregions were ablated simultaneously. This can be achieved, for example, by using different transgenic lines specific for the two subnuclei.[68] However, based on the calcium imaging results, we hypothesize the primary involvement of dHbM in homeostatic navigation. Furthermore, it would be interesting to understand if the dHb pathway is actively involved in sensorimotor transformation and/or acts as a global modulator, mostly through the serotoninergic and dopaminergic system, of brain dynamics[57,73]. Furthermore, it would be interesting to understand if the dHb pathway is actively involved in sensorimotor transformation and/or acts as a global modulator, mostly through the serotoninergic and dopaminergic system, of brain dynamics.[54,74]

Across biological systems, the modulation of forward movements vs. turns constitutes a simple and effective way of navigating the surroundings: bacteria coordinate their runs and tumbles,[13,42] *C. elegans* use runs and pirouettes,[3,17,75] fly larvae use runs and turns, and adult flies, as well as mammals, control exploration vs. exploitation strategies. Here, we show that fish do the same. To summarize, it appears that all organisms can exploit this behavioral strategy to successfully navigate in their surroundings, with the final goal of exploiting resources and avoiding homeostatic threats. In addition to this simple algorithm, further processing can be layered hierarchically to include more complex calculations in a species-specific way to increase efficiency. For example, in this study the dHb adds a sensorimotor memory, and, both in fish and other animals, more persistent representations may further aid navigation.[54,73] Comparative studies across model organisms will undoubtedly provide us with important insights as to how brain circuits solve this problem.

STAR★METHODS

Detailed methods are provided in the online version of this paper and include the following:

- KEY RESOURCES TABLE
- RESOURCE AVAILABILITY
  - Lead contact
  - Materials availability
  - Data and code availability
- EXPERIMENTAL MODEL AND SUBJECT DETAILS
  - Zebrafish husbandry
  - Transgenic animals
  - Enhancer trap line generation
- METHOD DETAILS
  - Experimental setups
  - Behavioral experiments
  - Lightsheet functional imaging
  - Data analysis and statistics
  - Behavior data analysis
  - Lightsheet data analysis
  - Neuron ablations

SUPPLEMENTAL INFORMATION

Supplemental information can be found online at https://doi.org/10.1016/j.cub.2023.12.030.

ACKNOWLEDGMENTS

We thank the German Research Foundation (DFG) for funding R.P. and I.G.K. (SPP 2205 – project 430156228). In addition, we acknowledge generous support from the Volkswagen Stiftung Life Initiative and the DFG under Germany's Excellence Strategy within the framework of the Munich Cluster for Systems Neurology (EXC 2145 SyNergy, identifier 390857198) to R.P. and the European research commission (ERC StG FlyContext) to I.G.K. The authors would like to thank Larissa Dillman and Lucia Rodriguez for the help with the behavioral experiments. We would also like to thank Thomas Frank, Florian Richter, and Luigi Petrucco for insightful discussions and comments on the manuscript and the Grunwald Kadow and Portugues labs for their input and encouragement.

AUTHOR CONTRIBUTIONS

V.P., I.G.K., and R.P. devised the project. V.P. built the experimental rigs and both V.P. and E.P. performed experiments and analyzed the data. Y.K.W. helped with the two-photon experiments and ablations. M.H. generated the transgenic fish line. All authors wrote the manuscript.

DECLARATION OF INTERESTS

The authors declare no competing interests.

Received: June 28, 2023
Revised: November 22, 2023
Accepted: December 11, 2023
Published: January 10, 2024

REFERENCES

1. Billman, G.E. (2020). Homeostasis: the underappreciated and far too often ignored central organizing principle of physiology. Front. Physiol. *11*, 200.
2. Goodman, L. (1980). Regulation and control in physiological systems: 1960–1980. Ann. Biomed. Eng. *8*, 281–290.
3. Garrity, P.A., Goodman, M.B., Samuel, A.D., and SenGupta, P. (2010). Running hot and cold: behavioral strategies, neural circuits, and the molecular machinery for thermotaxis in C. elegans and Drosophila. Genes Dev. *24*, 2365–2382.
4. Tominaga, M., and Caterina, M.J. (2004). Thermosensation and pain. J. Neurobiol. *61*, 3–12.
5. Craig, A.D., Chen, K., Bandy, D., and Reiman, E.M. (2000). Thermosensory activation of insular cortex. Nat. Neurosci. *3*, 184–190.
6. Nakamura, K., Nakamura, Y., and Kataoka, N. (2022). A hypothalamomedullary network for physiological responses to environmental stresses. Nat. Rev. Neurosci. *23*, 35–52.
7. Haesemeyer, M. (2020). Thermoregulation in fish. Mol. Cell. Endocrinol. *518*, 110986.
8. Hearings; Ninetieth Congress; Second Session. (1968). Thermal Pollution. Pollution, U.S. CSC. on P.W.S. on A. and W. (U.S. Government Printing Office).
9. Bicego, K.C., and Branco, L.G.S. (2002). Discrete electrolytic lesion of the preoptic area prevents LPS-induced behavioral fever in toads. J. Exp. Biol. *205*, 3513–3518.
10. Nelson, D.O., and Prosser, C.L. (1981). Temperature-sensitive neurons in the preoptic region of sunfish. Am. J. Physiol. *241*, R259–R263.
11. Le Goc, G., Lafaye, J., Karpenko, S., Bormuth, V., Candelier, R., and Debrégeas, G. (2021). Thermal modulation of zebrafish exploratory statistics reveals constraints on individual behavioral variability. BMC Biol. *19*, 208.
12. Herrera, K.J., Panier, T., Guggiana-Nilo, D., and Engert, F. (2021). Larval zebrafish use olfactory detection of sodium and chloride to avoid salt water. Curr. Biol. *31*, 782–793.e3.
13. Berg, H.C. (2000). Motile behavior of bacteria. Phys. Today *53*, 24–29.
14. Larsch, J., Flavell, S.W., Liu, Q., Gordus, A., Albrecht, D.R., and Bargmann, C.I. (2015). A circuit for gradient climbing in C. elegans chemotaxis. Cell Rep. *12*, 1748–1760.
15. Gomez-Marin, A., and Louis, M. (2012). Active sensation during orientation behavior in the Drosophila larva: more sense than luck. Curr. Opin. Neurobiol. *22*, 208–215.
16. Oteiza, P., Odstrcil, I., Lauder, G., Portugues, R., and Engert, F. (2017). A novel mechanism for mechanosensory-based rheotaxis in larval zebrafish. Nature *547*, 445–448.
17. Glauser, D.A. (2013). How and why *Caenorhabditis elegans* uses distinct escape and avoidance regimes to minimize exposure to noxious heat. Worm *2*, e27285.
18. Simões, J.M., Levy, J.I., Zaharieva, E.E., Vinson, L.T., Zhao, P., Alpert, M.H., Kath, W.L., Para, A., and Gallio, M. (2021). Robustness and plasticity in Drosophila heat avoidance. Nat. Commun. *12*, 2044.
19. Budick, S.A., and O'Malley, D.M. (2000). Locomotor repertoire of the larval zebrafish: swimming, turning and prey capture. J. Exp. Biol. *203*, 2565–2579.
20. Marques, J.C., Lackner, S., Félix, R., and Orger, M.B. (2018). Structure of the zebrafish locomotor repertoire revealed with unsupervised behavioral clustering. Curr. Biol. *28*, 181–195.e5.
21. Dunn, T.W., Mu, Y., Narayan, S., Randlett, O., Naumann, E.A., Yang, C.T., Schier, A.F., Freeman, J., Engert, F., and Ahrens, M.B. (2016). Brain-wide mapping of neural activity controlling zebrafish exploratory locomotion. eLife *5*, e12741.
22. Lovett-Barron, M., Chen, R., Bradbury, S., Andalman, A.S., Wagle, M., Guo, S., and Deisseroth, K. (2020). Multiple convergent hypothalamus-brainstem circuits drive defensive behavior. Nat. Neurosci. *23*, 959–967.
23. Bianco, I.H., Carl, M., Russell, C., Clarke, J.D., and Wilson, S.W. (2008). Brain asymmetry is encoded at the level of axon terminal morphology. Neural Dev. *3*, 9.
24. Bianco, I.H., and Wilson, S.W. (2009). The habenular nuclei: A conserved asymmetric relay station in the vertebrate brain. Philos. Trans. R. Soc. Lond. B Biol. Sci. *364*, 1005–1020.
25. Miyasaka, N., Arganda-Carreras, I., Wakisaka, N., Masuda, M., Sümbül, U., Seung, H.S., and Yoshihara, Y. (2014). Olfactory projectome in the zebrafish forebrain revealed by genetic single-neuron labelling. Nat. Commun. *5*, 3639.
26. Turner, K.J., Hawkins, T.A., Yáñez, J., Anadón, R., Wilson, S.W., and Folgueira, M. (2016). Afferent connectivity of the zebrafish habenulae. Front. Neural Circuits *10*, 30.
27. Jetti, S.K., Vendrell-Llopis, N., and Yaksi, E. (2014). Spontaneous activity governs olfactory representations in spatially organized habenular microcircuits. Curr. Biol. *24*, 434–439.
28. Bartoszek, E.M., Ostenrath, A.M., Jetti, S.K., Serneels, B., Mutlu, A.K., Chau, K.T.P., and Yaksi, E. (2021). Ongoing habenular activity is driven by forebrain networks and modulated by olfactory stimuli. Curr. Biol. *31*, 3861–3874.e3.
29. Ahrens, M.B., Li, J.M., Orger, M.B., Robson, D.N., Schier, A.F., Engert, F., and Portugues, R. (2012). Brain-wide neuronal dynamics during motor adaptation in zebrafish. Nature *485*, 471–477.
30. Kist, A.M., and Portugues, R. (2019). Optomotor swimming in larval zebrafish is driven by global whole-field visual motion and local light-dark transitions. Cell Rep. *29*, 659–670.e3.
31. Markov, D.A., Petrucco, L., Kist, A.M., and Portugues, R. (2021). A cerebellar internal model calibrates a feedback controller involved in sensorimotor control. Nat. Commun. *12*, 6694.
32. Severi, K.E., Portugues, R., Marques, J.C., O'Malley, D.M., Orger, M.B., and Engert, F. (2014). Neural control and modulation of swimming speed in the larval zebrafish. Neuron *83*, 692–707.
33. Dragomir, E.I., Štih, V., and Portugues, R. (2020). Evidence accumulation during a sensorimotor decision task revealed by whole-brain imaging. Nat. Neurosci. *23*, 85–93.
34. Haesemeyer, M., Robson, D.N., Li, J.M., Schier, A.F., and Engert, F. (2018). A brain-wide circuit model of heat-evoked swimming behavior in larval zebrafish. Neuron *98*, 817–831.e6.
35. Boulant, J.A. (2000). Role of the preoptic-anterior hypothalamus in thermoregulation and fever. Clin. Infect. Dis. *31* (suppl 5), S157–S161.
36. Osaka, T. (2004). Cold-induced thermogenesis mediated by GABA in the preoptic area of anesthetized rats. Am. J. Physiol. Regul. Integr. Comp. Physiol. *287*, R306–R313.
37. Morrison, S.F., Madden, C.J., and Tupone, D. (2014). Central neural regulation of brown adipose tissue thermogenesis and energy expenditure. Cell Metab. *19*, 741–756.
38. Morrison, S.F. (2016). Central neural control of thermoregulation and brown adipose tissue. Auton. Neurosci. *196*, 14–24.
39. Zhao, Z.D., Yang, W.Z., Gao, C., Fu, X., Zhang, W., Zhou, Q., Chen, W., Ni, X., Lin, J.K., Yang, J., et al. (2017). A hypothalamic circuit that controls body temperature. Proc. Natl. Acad. Sci. USA *114*, 2042–2047.
40. Dreosti, E., Vendrell Llopis, N., Carl, M., Yaksi, E., and Wilson, S.W. (2014). Left-right asymmetry is required for the habenulae to respond to both visual and olfactory stimuli. Curr. Biol. *24*, 440–445.
41. Fore, S., Acuña-Hinrichsen, F., Mutlu, K.A., Bartoszek, E.M., Serneels, B., Faturos, N.G., Chau, K.T.P., Cosacak, M.I., Verdugo, C.D., Palumbo, F., et al. (2020). Functional properties of habenular neurons are determined by developmental stage and sequential neurogenesis. Sci. Adv. *6*, eaaz3173.
42. Berg, H.C., and Brown, D.A. (1972). Chemotaxis in Escherichia coli analysed by three-dimensional Tracking. Nature *239*, 500–504.
43. Hernandez-Nunez, L., Chen, A., Budelli, G., Berck, M.E., Richter, V., Rist, A., Thum, A.S., Cardona, A., Klein, M., Garrity, P., et al. (2021).

Synchronous and opponent thermosensors use flexible cross-inhibition to orchestrate thermal homeostasis. Sci. Adv. *7*, eabg6707.

44. Gau, P., Poon, J., Ufret-Vincenty, C., Snelson, C.D., Gordon, S.E., Raible, D.W., and Dhaka, A. (2013). The zebrafish ortholog of TRPV1 is required for heat-induced locomotion. J. Neurosci. *33*, 5249–5260.
45. Robson, D.N. (2013). Thermal navigation in larval zebrafish.
46. Chen, X., and Engert, F. (2014). Navigational strategies underlying phototaxis in larval zebrafish. Front. Syst. Neurosci. *8*, 39.
47. Zhang, B.B., Yao, Y.Y., Zhang, H.F., Kawakami, K., and Du, J.L. (2017). Left habenula mediates light-preference behavior in zebrafish via an asymmetrical visual pathway. Neuron *93*, 914–928.e4.
48. Wee, C.L., Song, E.Y., Johnson, R.E., Ailani, D., Randlett, O., Kim, J.Y., Nikitchenko, M., Bahl, A., Yang, C.T., Ahrens, M.B., et al. (2019). A bidirectional network for appetite control in larval zebrafish. eLife *8*, e43775.
49. Corradi, L., Bruzzone, M., Maschio, M.D., Sawamiphak, S., and Filosa, A. (2022). Hypothalamic Galanin-producing neurons regulate stress in zebrafish through a peptidergic, self-inhibitory loop. Curr. Biol. CB *32*. 1497-1510.e5.
50. Kludt, E., Okom, C., Brinkmann, A., and Schild, D. (2015). Integrating temperature with odor processing in the olfactory bulb. J. Neurosci. *35*, 7892–7902.
51. Kuhara, A., Okumura, M., Kimata, T., Tanizawa, Y., Takano, R., Kimura, K.D., Inada, H., Matsumoto, K., and Mori, I. (2008). Temperature sensing by an olfactory neuron in a circuit controlling behavior of C. elegans. Science *320*, 803–807.
52. Biron, D., Wasserman, S., Thomas, J.H., Samuel, A.D.T., and SenGupta, P. (2008). An olfactory neuron responds stochastically to temperature and modulates Caenorhabditis elegans thermotactic behavior. Proc. Natl. Acad. Sci. USA *105*, 11002–11007.
53. Koide, T., Yabuki, Y., and Yoshihara, Y. (2018). Terminal nerve GnRH3 neurons mediate slow avoidance of carbon dioxide in larval zebrafish. Cell Rep. *22*, 1115–1123.
54. Petrucco, L., Lavian, H., Wu, Y.K., Svara, F., Štih, V., and Portugues, R. (2023). Neural dynamics and architecture of the heading direction circuit in zebrafish. Nat. Neurosci. *26*, 765–773.
55. McLean, D.L., and Fetcho, J.R. (2004). Ontogeny and innervation patterns of dopaminergic, noradrenergic, and serotonergic neurons in larval zebrafish. J. Comp. Neurol. *480*, 38–56.
56. Tan, C.L., and Knight, Z.A. (2018). Regulation of body temperature by the nervous system. Neuron *98*, 31–48.
57. Barrios, J.P., Wang, W.C., England, R., Reifenberg, E., and Douglass, A.D. (2020). Hypothalamic dopamine neurons control sensorimotor behavior by modulating brainstem premotor nuclei in zebrafish. Curr. Biol. *30*, 4606–4618.e4.
58. Lin, D., Boyle, M.P., Dollar, P., Lee, H., Lein, E.S., Perona, P., and Anderson, D.J. (2011). Functional identification of an aggression locus in the mouse hypothalamus. Nature *470*, 221–226.
59. Füzesi, T., Daviu, N., Wamsteeker Cusulin, J.I., Bonin, R.P., and Bains, J.S. (2016). Hypothalamic CRH neurons orchestrate complex behaviours after stress. Nat. Commun. *7*, 11937.
60. Lee, H., Kim, D.W., Remedios, R., Anthony, T.E., Chang, A., Madisen, L., Zeng, H., and Anderson, D.J. (2014). Scalable control of mounting and attack by Esr1+ neurons in the ventromedial hypothalamus. Nature *509*, 627–632.
61. Choi, J.H., Duboue, E.R., Macurak, M., Chanchu, J.M., and Halpern, M.E. (2021). Specialized neurons in the right habenula mediate response to aversive olfactory cues. Elife *10*.
62. Krishnan, S., Mathuru, A.S., Kibat, C., Rahman, M., Lupton, C.E., Stewart, J., Claridge-Chang, A., Yen, S.C., and Jesuthasan, S. (2014). The right dorsal habenula limits attraction to an odor in zebrafish. Curr. Biol. *24*, 1167–1175.
63. Amo, R., Aizawa, H., Takahoko, M., Kobayashi, M., Takahashi, R., Aoki, T., and Okamoto, H. (2010). Identification of the zebrafish ventral habenula as a homolog of the mammalian lateral habenula. J. Neurosci. *30*, 1566–1574.
64. Aizawa, H., Amo, R., and Okamoto, H. (2011). Phylogeny and ontogeny of the habenular structure. Front. Neurosci. *5*, 138.
65. Aizawa, H., Bianco, I.H., Hamaoka, T., Miyashita, T., Uemura, O., Concha, M.L., Russell, C., Wilson, S.W., and Okamoto, H. (2005). Laterotopic representation of left-right information onto the dorso-ventral axis of a zebrafish midbrain target nucleus. Curr. Biol. *15*, 238–243.
66. Agetsuma, M., Aizawa, H., Aoki, T., Nakayama, R., Takahoko, M., Goto, M., Sassa, T., Amo, R., Shiraki, T., Kawakami, K., et al. (2010). The habenula is crucial for experience-dependent modification of fear responses in zebrafish. Nat. Neurosci. *13*, 1354–1356.
67. Amo, R., Fredes, F., Kinoshita, M., Aoki, R., Aizawa, H., Agetsuma, M., Aoki, T., Shiraki, T., Kakinuma, H., Matsuda, M., et al. (2014). The habenulo-raphe serotonergic circuit encodes an aversive expectation value essential for adaptive active avoidance of danger. Neuron *84*, 1034–1048.
68. Chou, M.Y., Amo, R., Kinoshita, M., Cherng, B.W., Shimazaki, H., Agetsuma, M., Shiraki, T., Aoki, T., Takahoko, M., Yamazaki, M., et al. (2016). Social conflict resolution regulated by two dorsal habenular subregions in zebrafish. Science *352*, 87–90.
69. Palumbo, F., Serneels, B., Pelgrims, R., and Yaksi, E. (2020). The zebrafish dorsolateral habenula is required for updating learned behaviors. Cell Rep. *32*, 108054.
70. Cherng, B.W., Islam, T., Torigoe, M., Tsuboi, T., and Okamoto, H. (2020). The dorsal lateral habenula-interpeduncular nucleus pathway is essential for left-right-dependent decision making in zebrafish. Cell Rep. *32*, 108143.
71. Lee, A., Mathuru, A.S., Teh, C., Kibat, C., Korzh, V., Penney, T.B., and Jesuthasan, S. (2010). The habenula prevents helpless behavior in larval zebrafish. Curr. Biol. *20*, 2211–2216.
72. Okamoto, H., Cherng, B.W., Nakajo, H., Chou, M.Y., and Kinoshita, M. (2021). Habenula as the experience-dependent controlling switchboard of behavior and attention in social conflict and learning. Curr. Opin. Neurobiol. *68*, 36–43.
73. Heinze, S. (2023). Neuroscience: fish and fly headed in the same direction. Curr. Biol. *33*, R677–R679.
74. Marques, J.C., Li, M., Schaak, D., Robson, D.N., and Li, J.M. (2020). Internal state dynamics shape brainwide activity and foraging behaviour. Nature *577*, 239–243.
75. Hedgecock, E.M., and Russell, R.L. (1975). Normal and mutant thermotaxis in the nematode Caenorhabditis elegans. Proc. Natl. Acad. Sci. USA *72*, 4061–4065.
76. Vladimirov, N., Mu, Y., Kawashima, T., Bennett, D.V., Yang, C.T., Looger, L.L., Keller, P.J., Freeman, J., and Ahrens, M.B. (2014). Light-sheet functional imaging in fictively behaving zebrafish. Nat. Methods *11*, 883–884.
77. Davison, J.M., Akitake, C.M., Goll, M.G., Rhee, J.M., Gosse, N., Baier, H., Halpern, M.E., Leach, S.D., and Parsons, M.J. (2007). Transactivation from Gal4-VP16 transgenic insertions for tissue-specific cell labeling and ablation in zebrafish. Dev. Biol. *304*, 811–824.
78. Rohlfing, T., and Maurer, C.R. (2003). Nonrigid image registration in shared-memory multiprocessor environments with application to brains, breasts, and bees. IEEE Trans. Inf. Technol. Biomed. *7*, 16–25.
79. Štih, V., Petrucco, L., Kist, A.M., and Portugues, R. (2019). Stytra: an open-source, integrated system for stimulation, tracking and closed-loop behavioral experiments. PLOS Comput. Biol. *15*, e1006699.
80. Štih, V., Asua, D., Petrucco, L., Puppo, F., and Portugues, R. (2022). Sashimi. Zenodo. https://doi.org/10.5281/zenodo.5932227.
81. Namikawa, K., Murakami, K., Okamoto, T., Okado, H., and Kiyama, H. (2006). A newly modified SCG10 promoter and Cre/loxP-mediated gene amplification system achieve highly specific neuronal expression in animal brains. Gene Ther. *13*, 1244–1250.
82. Distel, M., Wullimann, M.F., and Köster, R.W. (2009). Optimized Gal4 genetics for permanent gene expression mapping in zebrafish. Proc. Natl. Acad. Sci. USA *106*, 13365–13370.

83. Hu, G., Goll, M.G., and Fisher, S. (2011). ΦC31 integrase mediates efficient cassette exchange in the zebrafish germline. Dev. Dyn. *240*, 2101–2107.

84. Harris, C.R., Millman, K.J., van der Walt, S.J., Gommers, R., Virtanen, P., Cournapeau, D., Wieser, E., Taylor, J., Berg, S., Smith, N.J., et al. (2020). Array programming with NumPy. Nature *585*, 357–362.

85. Virtanen, P., Gommers, R., Oliphant, T.E., Haberland, M., Reddy, T., Cournapeau, D., Burovski, E., Peterson, P., Weckesser, W., Bright, J., et al. (2020). SciPy 1.0: fundamental algorithms for scientific computing in Python. Nat. Methods *17*, 261–272.

86. Pedregosa, F., Varoquaux, G., Gramfort, A., Michel, V., Thirion, B., Grisel, O., Blondel, M., Prettenhofer, P., Weiss, R., Dubourg, V., et al. Scikit-learn: Machine Learning in Python. Mach. Learn. PYTHON.

87. Reback, J., McKinney, W., Jbrockmendel, Bossche, J.V.D., Augspurger, T., Cloud, P., Gfyoung, Sinhrks, Hawkins, S., Klein, A., et al. (2020). pandas-dev/pandas: Pandas 1.1.3. Version v1.1.3 (Zenodo).

88. Hunter, J.D. (2007). Matplotlib: A 2D graphics environment. Comput. Sci. Eng. *9*, 90–95.

89. Štih, Vilim, Petrucco, Luigi, Prat, Ot, Lavian, Hagar, Portugues, and Ruben. (2022). Bouter, version v0.2.0 (Zenodo).

90. Mathis, A., Mamidanna, P., Cury, K.M., Abe, T., Murthy, V.N., Mathis, M.W., and Bethge, M. (2018). DeepLabCut: markerless pose estimation of user-defined body parts with deep learning. Nat. Neurosci. *21*, 1281–1289.

91. Nath, T., Mathis, A., Chen, A.C., Patel, A., Bethge, M., and Mathis, M.W. (2019). Using DeepLabCut for 3D markerless pose estimation across species and behaviors. Nat. Protoc. *14*, 2152–2176.

92. Huang, K.H., Ahrens, M.B., Dunn, T.W., and Engert, F. (2013). Spinal projection neurons control turning behaviors in zebrafish. Curr. Biol. *23*, 1566–1573.

93. Stevens, J.C., and Choo, K.K. (1998). Temperature sensitivity of the body surface over the life span. Somatosens. Mot. Res. *15*, 13–28.

94. Paricio-Montesinos, R., Schwaller, F., Udhayachandran, A., Rau, F., Walcher, J., Evangelista, R., Vriens, J., Voets, T., Poulet, J.F.A., and Lewin, G.R. (2020). The sensory coding of warm perception. Neuron *106*, 830–841.e3.

95. Kunst, M., Laurell, E., Mokayes, N., Kramer, A., Kubo, F., Fernandes, A.M., Förster, D., Dal Maschio, M., and Baier, H. (2019). A cellular-resolution atlas of the larval zebrafish brain. Neuron *103*, 21–38.e5.

96. Prat, O., Petrucco, L., Štih, V., and Portugues, R. (2022). Comparing the representation of a simple visual stimulus across the cerebellar network. bioRxiv.

97. Bergemann, D., Massoz, L., Bourdouxhe, J., Carril Pardo, C.A., Voz, M.L., Peers, B., and Manfroid, I. (2018). Nifurpirinol: A more potent and reliable substrate compared to metronidazole for nitroreductase-mediated cell ablations. Wound Repair Regen. *26*, 238–244.

STAR★METHODS

KEY RESOURCES TABLE

REAGENT or RESOURCE	SOURCE	IDENTIFIER
Chemicals, peptides, and recombinant proteins		
Low melting point agarose	Invitrogen	Cat#16520-100
Nifurpirinol	Sigma	Cat#32439
Dimethyl sulfoxide (DMSO)	Sigma	Cat#D8418
Tricaine (Ethyl 3-aminobenzoate methanesulfonate)	Sigma	Cat#E10521
Experimental models: Organisms/strains		
4-7 days post fertilization; Danio rerio: Tg(elavl3:H2B-GCaMP6s)jf5; nacre-/-	Vladimirov et al.[76]	ZFIN ID: ZDB-ALT-141023-2
4-7 days post fertilization; Danio rerio: Tg(16715:Gal4);Tg(UAS:NTR-mCherry)c264; nacre+/- or -/-	This study; Davison et al.[77]	ZFIN ID: ZDB-ALT-070316-1
4-7 days post fertilization; Danio rerio: wild-type Tüpfel long-fin	N/A	ZFIN ID: ZDB-GENO-990623-2
Software and algorithms		
Computational Morphometry Toolkit (anatomical registration)	Rohlfing and Maurer[78]	https://www.nitrc.org/projects/cmtk/
Python 3.10	Anaconda, Inc.	https://www.anaconda.com/data-science-platform
Stytra (behavior acquisition software)	Štih et al.[79]	https://portugueslab.com/stytra/
Sashimi (lightsheet microscope acquisition software)	Štih et al.[80]	https://github.com/portugueslab/sashimi
Confocal microscope software	FV10-ASW	https://www.olympus-lifescience.com/en/downloads/detail-iframe/?0[downloads][id]=847249651
Custom python code for analysis and generating the figures in this study	This study	https://github.com/EmanPaoli/PalieriPaoli

RESOURCE AVAILABILITY

Lead contact

Further information and requests for resources, code and reagents should be directed to and will be fulfilled by the lead contact, Ruben Portugues (ruben.portugues@tum.de) or Ilona Grunwald Kadow (ilona.grunwald@ukbonn.de)

Materials availability

This study did not generate new unique reagents.

Data and code availability

Code used in the current study can be found here: https://github.com/EmanPaoli/PalieriPaoli

Data sets generated in this study can be found here: https://zenodo.org/records/10281421 (https://doi.org/10.5281/zenodo.10281421)

EXPERIMENTAL MODEL AND SUBJECT DETAILS

Zebrafish husbandry

All procedures related to animal handling were conducted following protocols approved by the Technische Universität München and the Regierung von Oberbayern. Adult zebrafish (Danio rerio) from Tüpfel long fin (TL) strain were kept at 27.5–28 °C on a 14/10 light cycle and hosted in a fish facility that provided full recirculation of water with carbon-, bio- and UV filtering and a daily exchange of 12% of water. Water pH was kept at 7.0–7.5 with a 20 g/liter buffer and conductivity maintained at 750–800 μS using 100g/liter. Fish

were hosted in 3.5 liter tanks in groups of 10 to 17 animals and fed the adults with Gemma micron 300 (Skretting USA) and live food (artemia salina) twice per day and fed the larvae with Sera micron Nature (Sera) and ST-1 (Aquaschwarz) three times a day.

All experiments were conducted on 5–7 dpf larvae of yet undetermined sex. The week before the experiment, one male and one female or three male and three female animals were left breeding overnight in a Sloping Breeding Tank or breeding tank (Tecniplast). The day after, eggs were collected in the morning, rinsed with water from the facility water system, and then kept in groups of 20–40 in 90 cm Petri dishes filled with Danieau solution 0.3x (17.4 mM NaCl, 0.21 mM KCl, 0.12 mM MgSO4, 0.18 mM Ca(NO3)2, 1.5 mM HEPES, reagents from Sigma-Aldrich) until hatching and in water from the fish facility afterwards. Larvae were kept in an incubator at 28,5°C and a 14/10 hour light/dark cycle, and their solution was changed daily. At 4 or 5 dpf, animals were lightly anesthetized with Tricaine 440 mesylate (Sigma-Aldrich) and screened for fluorescence under an epifluorescent microscope. Animals positive for GCaMP6s and mCherry fluorescence were selected for the imaging experiments.

Transgenic animals

The Tuepfel long-fin (TL) wild-type strain was used for freely swimming behavioral experiments. The nacre (*mitfa−/−*, lacking melanophores) transgenic zebrafish lines Tg(elavl3:GCaMP6s+/+), labelling all the neurons, and *Tg(16715:GAL4);Tg(UAS:NTR-mCherry))*, labelling the dorsal part of the Habenula, were used respectively for functional imaging experiments and chemogenetic ablations.

Enhancer trap line generation

The line Tg(pMH93-16715)a207 (referred as *Tg(16715:Gal4)*) was generated by random Tol-2 insertion of the enhancer trap vector pMH93 into a UAS-Kaede background. To this end purified DNA of pMH93 (40 ng/ul) was co-injected with purified Tol2 transposase RNA (100 ng/ul). Founders were identified based on tissue-specific expression of Kaede and stable lines were generated. The pMH93 vector contains a heatshock minimal promoter with two inserted NRSE sites to prevent non-neuronal expression[81] driving the Gal4 variant KalTA4.[82] The entire construct is flanked by attp sites to facilitate cassette exchange within the genome.[83] Relevant elements were assembled using PCR and restriction site-based cloning and the entire construct was subsequently inserted into a vector with Tol-2 transposase recognition sites via the Gateway system.

METHOD DETAILS

Experimental setups

Freely swimming rectangular arena (large arena)

The custom-made arena consists in a rectangular pool (200 × 40 × 3.5 mm^3) (Figure S1A) made of aluminum for homogeneous heat dispersal. The surface of the plate is taped, before each batch of experiments, with white tape (Tesa) to increase contrast and allow online tracking of fish. At both ends of the arena two Peltier modules (digikey, TEC-40-39-127) were fixed with thermal tape or thermal glue (Conrad Electronic). The arena is placed on a metal block which dissipates heat from the Peltier elements and whose temperature is constantly monitored (RS Components, Nr. 706-2743). The temperature is constantly monitored at both ends of the pool with waterproof thermocouples type Pt100 (RS Components, Nr.762-1134). Temperature is controlled by two independent TEC controllers (Meerstetter, TEC-1091). After about 5 min, the temperature of the water at both sides of the pool reaches the target temperatures (25 °C and 33 °C), which then remains constant over time. Water level is usually between 3–4 mm. Freely swimming larvae are monitored using a Ximea camera (MQ022MG-CM) at 110 fps, coupled with a macrolens (Navitar). The whole apparatus is placed in a light-tight box, illuminated with a homogeneous IR light emitted by a LED panel (Wilktop) placed on both sides, above the arena, spanning the entire small side of the setup.

Larvae were pipetted into the middle of the arena. However, the interval between the introduction of the animal in the arena and the start of the experiment might vary because of parameters adjustment in the tracking software.

Freely swimming square arena used for long temporal gradient experiment (small arena)

The arena consists of a square pool (40 × 40mm) (Figure 2D left) made of aluminum filled to a depth of 3–4 mm. A single 36 W Peltier element (50 x 50 x 3.5 mm) (digikey, TEC-40-39-127) is sandwiched between the heat sink and the arena and fixed with thermal tape (Conrad Electronic). Temperature is, therefore, changed homogenously in the entire volume of water (water level 3–4 mm). The Peltier is driven by a single TEC controller (Meerstetter, TEC-1091) and temperature is constantly monitored with a Pt100 thermocouple placed in the center of the arena (RS components, Nr. 891-9145). Homogenous illumination is provided from the side using IR light emitted by LED stripes (Solarox). Fish are tracked at 150 fps with a Ximea camera (MQ013MG-ON), coupled with a lens (Edmund Optics).

Perfusion system for head-embedded preparation under lightsheet microscope

We implemented a system where the head of the tethered fish is targeted with a constant flow at a rate of 1.5 ml/min of filtered fish water delivered through a needle (19 gauge) placed in front of the fish at an angle of 20–30° via a gravity-based 4-channels perfusion system (Figure 3A left). The needle is connected to an in-line solution heater/cooler (Warner Instruments, SC-20) to precisely regulate the temperature. Excess heat produced by the SC-20 Peltier is dissipated through a liquid cooling system (Koolance, Cat. EXT-1055). Water is constantly removed from the chamber to avoid overflowing using a small peristaltic pump controlled with an Arduino. The procedure ensures no changes in the water level (important for functional imaging purposes) and doesn't affect the behavior of the fish.

The desired temperature is set through a single channel temperature controller (Warner Instruments, CI−100) externally triggered by the computer handling the behavior protocol through a LabJack series U3-LV (LabJack). The controller also allows reading online the temperature inside the Heater/Cooler element and inside the chamber with a thermocouple which was placed immediately in front of the needle.

For salt experiments, we kept the temperature of the water flowing in the chamber at room temperature (24 °C) and we open/close a second valve connected to a reservoir with fish water at higher salt concentration (40 mM NaCl added to fish water). The switch is mediated by solenoid valves pinching the tubing and whose state is controlled by a ValveLink 8.2 perfusion controller (Automate Scientific, 04-08-zdv) timed with the behavior protocol through an Arduino 1 (Arduino). A perfusion pencil tip combining 4 tubes into a single tip (AutoMate Scientific, 04-08-250) placed between the solenoid valves and the inline heater/cooler (switched off for this particular experiment) ensures rapid liquid volume exchange.

Behavioral experiments

All the experiments where behavior was recorded were run from 10:00 h to 20:00 h. Since all experiments were carried out in darkness, we removed the fish from the incubator at least 2 hours before testing.

Spatial gradient in the large arena

For controlling the thermal gradient stability, on top of having the temperature constantly monitored at both ends of the pool by waterproof thermocouples, we divided the chamber into 10 bins of 2 cm each and we measured the temperature in each bin with a digital thermometer at the beginning and at the end of each experiment. Individual fish were then transferred to the arena and their behavior was monitored in the gradient for 15 minutes. Larvae were placed in the pool after the target temperatures (24 °C and 33 °C) were reached. The warmer side was randomized across experiments.

Long temporal gradient in the small arena and for head-restrained preparation

This protocol was presented to both head-restrained larvae under the lightsheet microscope and freely swimming larvae in the small square pool. The experiments lasted a total of 60 minutes. The temperature was changed in the whole arena from 24 °C to 30 °C and then back to 24 °C with 2 °C steps lasting 2 minutes each. Each fish was presented with three repetitions of this ramp stimulus. At the end and at the beginning of each ramp the fish had 5 minutes where the temperature was kept constant at 24 °C. The temperature was monitored online.

Multimodal short temporal gradient for head-restrained preparation

Each head-restrained larval zebrafish we tested with this protocol was presented with a salt followed by a temperature session or vice versa. Before starting the experiment, fish were placed under the microscope with the laser on and fish water flowing for five minutes to let them habituate. The protocol comprised 5 repetitions of the same stimulus block. Each stimulus block lasted 480 s. During the experiment, the room temperature was kept at 24 °C, and the water was flowing at a low rate (<1.5 mL/minute). The overall protocol is described below. After 40 seconds, we induced a change in temperature or salinity (depending on the session type) for the next 40 seconds. For the temperature session, the Peltier element was set to a target temperature of 27 °C, resulting in an effective temperature increase of +0.2 °C while for the salt session we opened a second valve and released a high salinity solution. Afterward, there was a 90 second pause to allow the temperature or salinity to return to the baseline level. The second part of the experiment began with 50 seconds of temperature increase (with target temperature of 27 °C) or 40 seconds of an increase in salinity followed by a 10-second pause. Then, for the next 40 seconds, the target temperature of the Peltier was set to 29 °C (effective temperature increase of +0.4 °C), or there was another 40-second increase in salinity. The block ended with 140 s of pause (experiment 4, Figure 3B right). The length of the pulses and pauses was chosen to obtain the same stimulus profile across modalities and to not have an accumulation of temperature and salinity in the chamber over time (Figure S4F, G). To this end, we previously measured the conductance in water with an Arduino and we matched change in medium conductance (proportional to salinity concentration) from baseline to what we recorded with the thermocouple in the chamber. Randomization of double and single pulses was not possible due to accumulation phenomena in the case of two double pulses coming one after the other.

Lightsheet functional imaging

Lightsheet microscope

For our experiments we used a custom-built microscope with two excitation scanning arms placed at 90° from each other. A laser beam coming from a 473 nm laser source (Cobolt) is split and directed into the two arms. In both arms, the laser beam gets expanded by a telescope before being focused through a glass coverslip on the fish. By scanning at 800 Hz the beam on the horizontal plane we generated the excitation lightsheet. The brain of the fish is targeted from the side and from the front giving access to the entire brain at a single-cell resolution. The emitted fluorescence was collected through a water immersion objective (Olympus, Japan), mounted on a piezo (Piezosystem Jena, Germany) and focused on a camera (Orca Flash v4.0, Hamamatsu Photonics K.K., Japan) with a tube lens (Thorlabs, USA). For further details refer to.[31]

The piezo, galvanometric mirrors and the triggering of the camera was controlled by Sashimi[80] a custom-written python software developed in the lab. The lightsheets and the collection objective were synchronously oscillating along the vertical axis with a frequency of 2.0 Hz, covering in depth around 250 μm. Frames were acquired at equally spaced intervals along the volume with a spacing of 9–10 μm.

Embedded (head-restrained) preparation

For lightsheet experiments 6–7 dpf fish are placed in 2.2% low-melting point agarose (Thermofisher) in a chamber optimized for our lightsheet microscope.

The chamber is filled with filtered fish water and agarose is removed along the optic path of the lateral and frontal laser beams (to prevent scattering), around the tail of the animal, to enable movements of the tail and around the mouth and nose. After embedding, fish are left recovering overnight before the imaging session. Before starting the imaging, light tapping on the side of the chamber is used to select the most active fish for the experiment.

The tail of the fish was tracked using an infrared source (RS Components) illuminating the larva from above. A camera (Ximea) was focused on the fish from below and through the transparent bottom of the lightsheet chamber and acquired frames at 400 Hz. Tail movements were tracked online using Stytra.[79]

Data analysis and statistics

All analysis were performed using Python 3.8 and relevant Python libraries for scientific computing, like numpy,[84] scipy[85] and scikit-learn.[86] Dataframes and dataframe manipulations were performed with pandas library.[87]

The figures were produced using matplotlib.[88] For statistical analysis, unless otherwise stated, we used the non-parametric Mann-Whitney U test for unpaired comparisons (*mannwhitneyu* from scipy).

n.s.: not significant, p-value > 0.05
*: p-value 0.05-0.01
**: p-value 0.01–0.001
***: :p−value < 0.001

Behavior data analysis

Tracking and general preprocessing

For both WT freely swimming and head-restrained experiments the relevant parameters were tracked online using Stytra.[79] For each experiment metadata with all the relevant information were saved in the same folder of the behavior and the stimulus file. Most of behavioral preprocessing (like extraction of swim events) was performed using the python package Bouter.[89] Briefly, swim events were segmented putting a threshold on the velocity of the centroid. We, then, calculated the angle turned as the difference in heading between the beginning and the end of a swim.

For experiments with nacre (mitfa−/−) transparent fish we recorded an mp4 video, extracted fish centroid with Deeplabcut 2.0,[90,91] and then preprocessed with custom-made scripts. In particular, we segmented swim events using velocity of the centroid (1mm/s for swim onset) and extracted angle turned by fitting a linear vector using xy trajectories before and after a swim and measuring the signed angle between them.

For head-restrained experiments, we computed the standard deviation of the tail angle trace in a rolling window of 50 ms. Then, using a threshold of 0.1, we found swim onset. The sum of the tail angle during the first 70 ms of a swim has been shown to approximate well the angle turned by a freely swimming fish[33,92]and was therefore used to define angle turned during swims.

We set a threshold of ± 0.52 radians (30 degrees) and we respectively classified swim events (both for freely-swimming and head-restrained experiments) as right, left and forward swims. By convention, negative sign of angle turned is toward the left.

Extraction of relevant behavioral parameters for large arena experiment

We flipped horizontally the trajectories when the warm side was on the right. Therefore, by convention, the unpleasant stimulus is always on the left. To express the coordinates of the fish in terms of the temperature experienced we quadratically interpolated temperature calibrations taken every 2 cm in the arena before and after each batch of experiments.

Since all experimental conditions except for the WT preferred a higher temperature, we decided to express the currently experienced temperature as a function of the absolute distance from the fish setpoint. This setpoint was separately computed for WT, chemogenetic experiments and 2-photon ablation experiments. As shown by Figures S5B and 6C, no difference in setpoint was found between experimental and control groups, indicating that this shift in setpoint is independent from the region ablated.

The point of the analysis was to see whether fish behavior was modulated by sensory history and previous motor choices. To this end, we computed, for each swim, the following parameters:

- Angle turned during the swim event (see previous paragraph).
- Experienced temperature before and after swim
- Difference in temperature brought by the previous swim ($swim_{-1}$), if the interswim interval was $\leq$2 seconds. In the work, we refer to this variable as sensory context.
- Difference in temperature brought by the second-to-last swim ($swim_{-2}$), if the interswim interval between $swim_{-1}$ and $swim_{-2}$ was $\leq$ 2 seconds. In the work, we refer to this variable as past sensory context.

Sensory context and past sensory context were further classified in WCxt (worsening context), ICxt (improving context) and NCxt (no context). For such classification, we used a conservative threshold of 0.13 °C, which we posit to be the thermal sensitivity in the temporal domain.[93,94]

Fish that swam less than 1/3 Hz during an experiment were excluded from further analysis.

Increase in turn fraction index

To assess whether a fish would be more prone to turn when it experienced a WCxt we took all the swim events happening at least 1 °C away from setpoint and we looked at the fraction of turns happening in a WCxt and in an ICxt. Then, we took the difference between the two contexts.

In this analysis, we did not use the swim events in a NCxt. However, given the shape of our arena and gradient, it was common for the fish to use more than one movement to reverse a WCxt in an ICxt or vice versa (Figure 2G), therefore going through movements during which the temperature did not change (Figure 2I). Despite this, fish still proved efficient homeostatic navigation. To account for this, we repeated the previous analysis, but this time, we selected swims when sensory context was NCxt but past sensory context was either WCxt or ICxt.

Motor correlation index

In order to investigate if fish strengthen directional correlation during WCxt we selected all swims during such sensory context and further selected swims that were preceded by a turn (either left or right). Finally, we computed the theta swim normalized by the direction of the previous turn (we flipped the sign of current swim if previous turn was toward the left), such that if the sign is positive it means that fish moved ipsilateral respect to previous direction, contralateral otherwise.

U-maneuvers

In order to extract U-maneuvers, we selected sequences of six consecutive swim and computed the absolute amount of reorientation. If this number exceeded 100°, we considered that sequence a U-maneuver. We further selected U-maneuvers where the first swim was in a WCxt. Finally, we averaged the ΔTemperature experienced during each swim in the sequence.

Increase in turn fraction and motor correlation in open-loop head-restrained and freely swimming (small arena)

In these experiments, we tested whether the direction of change (WCxt vs ICxt) was enough to modulate the reorientation probability and directional correlation even if the fish had no control over the experienced temperature change.

For data analysis, we considered two main parts: when the temperature was moving away from 24 °C (24 °C to 28 °C = WCxt) and when it was moving towards 24 °C (28 °C to 24 °C = ICxt). We excluded the step at 30 °C from the analysis. We next computed the increase in turn fraction and motor correlation in the same way as we did for experiment 1 (see "Increase in turn fraction index" and "Motor correlation index").

Coefficient of dispersion

To test whether ablated fish were less able to stay around their setpoint we calculate the coefficient of dispersion:

$$CoD = \frac{\sum_{i}^{N} |x_i - x_m|}{N x_m}$$

where x_i is the preferred temperature of each fish, x_m is the median preferred temperature of the population and N is the total number of fish.

Lightsheet data analysis

Lightsheet imaging data preprocessing

Data were saved in hdf5 format. To preprocess functional imaging data we used the package fimpy (https://github.com/portugueslab/fimpy). For alignment (function *align_volumes_with_filtering*) and ROI extraction (function *correlation_map* and *grow_rois*), we used similar pipeline used in[31] (see "Whole-brain functional imaging data analysis"). Since planes were spaced by ~10 μm, ROIs detected across planes were not merged. Once the ROIs were identified, we generated an ID ROI stack: a matrix with the same shape of the lightsheet data where to each pixel was assigned a scalar value corresponding the ID of a single ROI. After ROI detection we removed spurious ROIs detected outside the brain by manually drawing a mask. We further removed all ROIs detected in the olfactory epithelium since it was imaged only in a small fraction of fish and it was prone to many movement artifacts. Alignment was performed independently for both temperature and salt session while ROI extraction only for temperature. After alignment, we additionally computed an anatomical stack by averaging fluorescence throughout the experiment for both sessions (anatomical stack).

ROI segmentation across sessions

Registration across sessions was performed by finding an affine transformation matrix semi-manually. This was done by finding ~15 corresponding single isolated neuronal nuclei in the temperature (used as reference) and the salt session anatomies and computing a least-squares fit of a 12-parameter affine transform matrix. Once found, we applied the inverse transformation (from the temperature to the salt session space) to the ID ROI stack computed in the temperature session in order to extract fluorescence activity from the same neuron in the salt session.

Anatomical registration and region segmentation

Image registration was performed using the free Computational morphometry Toolkit (CMTK – http://www.nitrc.org/projects/cmtk).[78] First, we choose one of the anatomical stacks as the initial reference brain, and non-affine volume transformations were computed to align each fish's anatomical stack to this reference stack using the affine and warp functions.[32] After this step, we averaged all the aligned anatomical stack from all fish in order to obtain an intermediate reference stack. We finally repeated the fish-wise alignment on the intermediate reference stack. These transformations were then used to transform individual ROIs from each fish into

the frame of reference of the final reference brain, allowing us to compare the anatomical location of ROIs from different fish. Finally, we built an internal atlas by manually defining anatomical regions using clear anatomical landmarks and by looking at the Max Planck Zebrafish Brain Atlas (https://mapzebrain.org).[95]

Describing temperature sensory responses

Raw traces were first smoothed with a median filter of size 1.5 s (function *medfilt*). Then, we cropped all traces from the beginning to the end of each trial (single + double pulse), z-score each of them, and performed an average response per each ROI (Trial trigger average or TTA). In addition, we computed the average correlation (reliability index) of the responses across all individual trials.[96] With the reliability index, we were able to quantify the responsiveness of each ROI to the temperature stimulation independently from each specific response profile. We classified each ROIs as ''reliable'' if the aforementioned index was higher than 0.3 and further analyzed only this subset of ROIs. This procedure allowed us to keep only neurons reliable across trials. In order to further screen for neuronal responses that were also reliable across animals, we cross-correlated (Pearson correlation) each TTA with all the TTAs of all the other fish and kept only neurons with a coefficient higher than 0.65 with at least one TTA of all the rest of the fish. At the end, we pooled together all the TTAs that passed these screenings. We then performed PCA and projected each TTA on the first two PCs (cumulative explained variance 65%) so that each point in the principal component space was a TTA. Finally, we performed k-means clustering and we set the number of clusters (k parameter) to 3. This number, was chosen by looking at the Davies Bouldin score (*davies_bouldin_score*), lower values of this score indicate better clustering. Clustering quality was also checked by repeating the procedure with different centroids initializations. Regional percentages of different clusters were computed using our internal atlas.

Visualization of whole brain maps

In order to generate whole brain maps displayed in the current work we used either a scatter plot or a density map. For the scatter plot (Figure 3J), color of each dot (representing a ROI) was decided based on cluster identity while transparency was proportional to the local density within a sphere of 30 μm radius. For the density maps (Figures 4A, 4F, S4H, S5E and S5G), we initialized a zero array with the same size of our internal reference brain (see ''Anatomical Registration and region segmentation''). We then increased by one (+1) pixel values corresponding to a spherical region of 15 μm around each selected ROI. For the visualization, we used a sum projection along the three main anatomical axis.

Multimodal neurons

In order to find multimodal neurons, we first selected all ROIs that reliably responded during both temperature and salt session (threshold: 0.3). The anatomical distribution of these ROIs is shown in Figure S5G. We then cross-correlated (Spearman correlation) the TTA of the two sessions and, for each ROI, generated a null-distribution by repeating the cross-correlation with circular-shuffled versions of the TTAs. Using the real correlation and the null-distribution we computed a p-value for each ROI. We considered a ROI multimodal if such correlation was higher than 0.3 and the p-value lower than 0.025.

We, then, applied a spatial constrain on the generated density maps shown in Figures 4F and S5G such that we show only regions with an overlap of at least 5 and 10 ROIs respectively.

Swim triggered analysis

The analysis aimed to identify neurons whose fluorescence increased after a swim event. First, we selected swim events temporally space 2 seconds from the precedent and 10 seconds from the next. Then we split swims according to the angle turned in order to classify them as left, right or forward swims. The threshold used for classification was the same as used for other experiments (±30 degrees). For each fish, the number of swims per each category was at least 3. We then cropped each ROI around swim onset (from -2 to +10s from swim onset). For each ROI, we computed 3 reliability indexes, one for each swim category. We used the 90th percentile of the distribution created by taking the maximum value among the three reliability indexes of all ROIs to find a global threshold, within fish, used to define if a ROI was motor responding and specific to one of the three swim categories. A ROI in order to be selected needed to have one of the three reliability indexes higher than the global threshold and the other two lower than that one so that each neuron was univocally classified as either left, right or forward tuned.

For the map shown in Figure 4A, we then pooled all the left-, right-swim (flipped along the rostro-caudal axis) and forward-swim tuned ROIs coming from all fish and computed the density map as described in ''Visualization of whole brain maps''. The percentage of motor ROIs was computed using our internal atlas. Finally, Figure S5E show only the left-swim and right-swim tuned ROIs on the left and right side, respectively.

Neuron ablations

Chemogenetic ablations

To perform targeted ablation of Hb, we employed nitroreductase (Ntr) / nifurpirinol (NFP) pharmaco-genetic approach.[49,97] Animals expressing Ntr in a cell population of interest were treated with prodrug NFP. Ntr converts NFP into a cytotoxic DNA cross-linking agent leading to death of cells of interest. Nirfurpirinol is, like metronidazole (MTZ), another nitroaromatic antibiotic and it has been shown to reliably trigger cell-ablation at concentrations 2000 fold-lower than MTZ.[97] We used the line *Tg(16715:Gal4); Tg*(*UAS:Ntr-mCherry*), which restricts expression in the dorsal Hb (see Figure S6A) and we crossed it with TL wild-type fish. Fish were screened with an upright fluorescence dissecting microscope (Leica, M165 FC) for red fluorescence, at 4 dpf.

MCherry-positive *Tg(16715:Gal4); Tg(UAS:Ntr-mCherry +/-)* fish were tested at 5dpf in the freely swimming rectangular arena (Genetic control). In the evening, 5dpf mCherry-positive *Tg(16715:Gal4); Tg(UAS:Ntr-mCherry +/-) f*ish and mCherry-negative *Tg(16715:Gal4); Tg(UAS:Ntr-mCherry -/-)* (Treatment control) were taken from their Petri dish minimizing the amount of water transferred and placed into a new 9 cm Petri dish filled with 40 ml of 0.2% DMSO (dimethyl sulfoxide) to increase tissue permeability, 5 μM

nifurpirinol (diluted 1:500 from stock 2.5 mM) and fish water. Solution preparation and fish transfer happened in darkness. Larvae were then placed in the incubator at 28 °C for 16 h in a black box to prevent the inactivation of the drug. The next morning fish were rinsed 3 times to thoroughly remove the NFP and DMSO and were left to recover for one day in fresh fish water.

Positive Hb fish treated with NFP (Experimental group) and negative Hb fish treated with NFP (Treatment control) were then tested at 7 dpf in the freely swimming rectangular arena. After the experiment fish were inspected individually under the fluorescence dissecting microscope to ensure absence of mCherry fluorescence.

The efficiency of Hb ablations was further evaluated by randomly selecting, each time we ran experiments on a different batch of fish, 5–6 mCherry-positive nacre (mitfa−/−) larvae that were imaged under a confocal microscope (Olympus FV1000) before ablations at 5 dpf and then after ablation at 6 dpf and again at 7 dpf (see Figure S6B). The rationale of the last step at 7 dpf was to confirm that the process of ablation keeps progressing up to 48 h after treatment with NFP.

Laser-mediated cell ablations

At 5 dpf *Tg(elavl3:GCaMP6s+/+) (mitfa−/−)* fish were mounted in 1.5 % agarose, anesthetized with 1x Tricaine (168 mg/L) directly added to fish water and placed under a custom-made 2-photon microscope. For the microscope design and details refer to.[54] To test the involvement of the PoA in thermal navigation we set to bilaterally ablate this structure. The PoA was identified based on its anatomical location and clear anatomical landmarks. Before the experiment, we acquired for each fish a 100 μm stack of the areas we intended to target (see Figure S6A Pre). Then we used galvo-based scanning to focus 800 nm on a small group of cells at either side of the midline. Even though we target a relatively small group of neurons (5–6 somas) the produced damage extended beyond the targeted area to the nearby cells. The laser power was 130 mW power measured at the objective back aperture. We used a protocol where we targeted the group of cells for 200 ms with a 500 ms of interval repeated three times. A Python script automatically controlled both the shutter and exposure time. Neurons were considered successfully ablated when the fluorescence sharply increased, and the nuclei looked irregular and fragmented (see Figure S6A Post). At this point, we took another anatomical image to monitor the localization and extent of the ablation. If the fluorescence of the neurons did not increase or the procedure created air bubbles in the tissue, the fish was not used for subsequent experiments. In control fish, we applied the same protocol used for the PoA to the optic tectum (OT) (Figure S6A, bottom row). The OT was the only brain region that did not reliably or strongly respond to our temperature stimulus (see Figures 3J and S4H). Successfully ablated and control fish were freed from the agarose, returned to a petri dish with fresh fish water and provided with Sera Micron (Sera). Fish were tested 24–48 hours later at 7 dpf. For some fish an additional anatomical stack was acquired after 48 hours to further monitor the scars.